Rudolph Norman-Elvenich

Effective Low-Energy Hamiltonians for Correlated Transition Metal Compounds

DIPLOMARBEIT

zur Erlangung des akademischen Grades
Diplom-Ingenieur

Diplomstudium Technische Physik

Technische Universität Graz

Betreuer:
Univ.-Prof. Dr. Enrico Arrigoni
Mitbetreuer:
Mag. DDr. Liviu Chioncel
Institut für Theoretische Physik - Computational Physics

Graz, Februar 2010

Abstract

Effective low-energy Hamiltonians play an important role in theoretical solid state physics. They have the advantage to describe the important physics of a quantum-mechanical system in a reduced Hilbert space.

In this thesis, we discuss the so-called Löwdin downfolding technique as a method to construct such Hamiltonians. It consists in effectively integrating out some of the bands, yielding a simpler model for the remaining states.

In a first part, we test the approach by applying it to different tight-binding multi-band models for CuO_2-planes in High Temperature Superconductor materials.

As a practical application, we carry out the method to the transition metal compound $SrVO_3$ in which the $V - 3d - t_{2g}$ orbitals are identified as the essential ones around the Fermi level.

In a further step, we add the electron Coulomb interaction to the model and construct an interacting three-band Hubbard Hamiltonian for the correlated material $SrVO_3$. We solve the model within the Variational Cluster Approach (VCA). Results show a material close to the metal-insulator transition.

Kurzfassung

Effektive niedrig-Energie Hamiltonoperatoren spielen eine wichtige Rolle in der theoretischen Festkörperphysik. Sie haben den Vorteil, die relevante Physik eines quantenmechanischen Systems in einem reduzierten Hilbertraum zu beschreiben.

In dieser Diplomarbeit wird die sogenannte Löwdin downfolding Technik als eine Methode vorgestellt um solche Hamiltonoperatoren zu erzeugen. Sie besteht darin, einige der Bänder effektiv auszuintegrieren um ein einfacheres Modell für die übrigen Zustände zu erhalten.

In einem ersten Teil der Arbeit wird diese Näherungsmethode getestet, indem sie auf verschiedene tight-binding multi-Band Modelle für die CuO_2-Ebenen in Hochtemperatursupraleitern angewendet wird.

Danach wird als praktische Anwendung diese Methode für die Übergangsmetallverbindung $SrVO_3$ durchgeführt, in der sich die $V-3d-t_{2g}$-Orbitale als die relevanten herausstellen, die sich nahe der Fermienergie befinden.

In einem weiteren Schritt wird die Coulombwechselwirkung dem Modell hinzugefügt und ein wechselwirkender drei-Band Hubbard-Hamiltonoperator für das stark korrelierende Material $SrVO_3$ erzeugt. Dieses Modell wird mittels der Variationellen Cluster Strungstheorie (VCA) gelöst. Die Ergebnisse zeigen ein Material nahe des Metall-Isolator-Überganges.

Contents

Chapter 1

Introduction

In theoretical solid state physics, quantum-mechanical systems are described by Hamiltonians in a certain Hilbert space representing the degrees of freedom considered for this system. In general, when large energy scales are well separated from the low-energy sector situated around the Fermi Energy, low-energy effective Hamiltonians can be constructed having the advantage of being formulated in a smaller Hilbert space. The price for this simplification is often that both the Hamiltonian and the operators take a form that is more complicated than that of the original theory. Standard methods used to obtain low-energy Hamiltonians are, for example, the perturbative Brillouin-Wigner type methods, the canonical transfromation and the Löwdin diagonalization. All these methods lead to similar results and are frequently applied in theoretical solid state physics to describe strong correlated materials. In these systems, an important role is played by the Coulomb electron-electron interactions. Therefore suitable methods that go beyond mean-field theory have to be adopted. A large class of strongly correlated materials are transition metal compounds, containing atoms of the d-block of the periodic system of elements. The unfilled d-orbitals contribute to a number of interesting properties such as high-temperature superconductivity and metal-insulator transitions.

At the beginning of this thesis, the general theory for the Löwdin downfolding technique is presented. The first part of this diploma work was devoted to develop a program to realize this method numerically and to test it on different examples. We apply it to describe the copper-oxide planes in two representants of high temperature superconducting materials, in partic-

ular the single layer compound $La_{2-x}Sr_xCuO_4$ and the bilayer $YBa_2Cu_3O_7$. Starting from a multi-orbital tight-binding model we perform downfolding to effective three and one-band Hamiltonians. We investigate the method concerning accuracy and dependence on the parameters.

Chapter three presents the basics of the Hubbard model. Several levels of approximations are discussed, the atomic limit and the Hubbard-I approximation are presented in detail. As an improvement of the latter, the Cluster perturbation Theory (CPT) is introduced. Finally, the Variational Cluster approach (VCA) is presented as an extension of CPT.

The last chapter describes the combination of an ab-initio and many-body calculation with an application to the strongly correlated material $SrVO_3$. First, we construct a three-band low-energy Hamiltonian for the $V-3d-t_{2g}$ orbitals using the NMTO downfolding method, to which local Coulomb interactions are added. We then solve the interacting Hamiltonian using the Variational Cluster Approach. This chapter contains preliminary results, which are discussed and compared with previous results obtained by other approximations such as Dynamical mean Field Theory and with experimental data.

As an overall conclusion of the present thesis we can say that the combination of the downfolding technique with many-body calculation provides a powerful method to describe correlation effects in a realistic way. The quality of the results obviously depend on the approximations one makes in deriving the low-energy Hamiltonian as well as in solving the many-body problem. It is expected that in the future the computational development would trigger the improvement of both this techniques, such that the combination of the electronic structure and many-body physics would be developed towards a more quantitative description of correlated materials.

Chapter 2

Construction of effective low-energy models

In this chapter, the Löwdin downfolding method [1] is presented. For a given model Hamiltonian it reduces the number of degrees of freedom creating an effective Hamiltonian in a smaller Hilbert space. The purpose of this part of the thesis is to test this method on 'toy'-models. We start from a tight-binding model restricted to a certain number of bands N_1, and reduce the number of bands to N_2, ($N_2 < N_1$). We discuss the results of the downfolding procedure concerning accuracy and dependence on the parameters. In particular, tight-binding Hamiltonians are derived for the energy bands of a CuO_2-plane, which is the important feature of high-temperature superconducting materials (HTSC) [2]. We perform downfolding for the single layer compound $La_{2-x}Sr_xCuO_4$ from three to one band, which is presented in Sec. 2.2, whereas for the bilayer $YBa_2Cu_3O_7$ we do downfolding from eight band to three and one (Sec. 2.3). For the latter example, results are also compared to the low-energy bands presented in the work of Andersen et al. [3].

2.1 The downfolding technique

The idea of the Löwdin downfolding method [1, 4, 5, 6, 7] is to divide the Hilbert space of a quantum-mechanical system in two subspaces, a subspace A, containing the states one is interested in, and another subspace B, containing the rest of the states belonging to the full system. Those states will

be integrated out (downfolded), yielding an effective Hamiltonian restricted to the remaining states. The following derivation follows the paper by E. Zurek et al. [6].

The Hamiltonian of the full system, H, a hermitian matrix of dimensions $N_1 \times N_1$, can be written in blocks of four submatrices:

$$H = \begin{pmatrix} H^{(A)} & V \\ V^\dagger & H^{(B)} \end{pmatrix} \tag{2.1}$$

where $H^{(A)}$ is a $N_2 \times N_2$ matrix in the subspace A, and $H^{(B)}$ a $N_3 \times N_3$ matrix in the subspace B. Of course, $N_1 = N_2 + N_3$ is valid. The matrices V and $V^\dagger$ are of dimensions $N_2 \times N_3$ and $N_3 \times N_2$ respectively, and describe the overlap between the two subspaces. To get the energy eigenvalues ε, the Schrödinger equation has to be solved:

$$H\vec{U} = \varepsilon\vec{U} \tag{2.2}$$

The partition of the Hilbert space concerns of course in the same way the eigenvectors

$$\vec{U} = \begin{pmatrix} \vec{U}^{(A)} \\ \vec{U}^{(B)} \end{pmatrix}, \tag{2.3}$$

so that the eigenvalue equation can be written in the form

$$\begin{pmatrix} H^{(A)} & V \\ V^\dagger & H^{(B)} \end{pmatrix} \begin{pmatrix} \vec{U}^{(A)} \\ \vec{U}^{(B)} \end{pmatrix} = \varepsilon \begin{pmatrix} \vec{U}^{(A)} \\ \vec{U}^{(B)} \end{pmatrix}, \tag{2.4}$$

and divided into a system of two equations

$$H^{(A)}\vec{U}^{(A)} + V\vec{U}^{(B)} = \varepsilon\vec{U}^{(A)} \tag{2.5}$$

$$V^\dagger\vec{U}^{(A)} + H^{(B)}\vec{U}^{(B)} = \varepsilon\vec{U}^{(B)}. \tag{2.6}$$

This system of equations can be solved easily. We are interested in the A-part of the system. From Eq. (2.6) one obtains

$$\vec{U}^{(B)} = (\varepsilon\mathbb{1}^{(B)} - H^{(B)})^{-1}V^\dagger\vec{U}^{(A)}, \tag{2.7}$$

and by inserting this in Eq. (2.5) one gets the following equation for the dimensions of interest A only:

$$\underbrace{\left(H^{(A)} + V\left(\varepsilon\mathbb{1}^{(B)} - H^{(B)}\right)^{-1} V^{\dagger}\right)}_{H_{\text{eff}}} \vec{U}^{(A)} = \varepsilon\vec{U}^{(A)} \tag{2.8}$$

One can now define an effective, downfolded Hamiltonian:

$$H_{\text{eff}}(\varepsilon) = H^{(A)} + V\left(\varepsilon\mathbb{1}^{(B)} - H^{(B)}\right)^{-1} V^{\dagger} \tag{2.9}$$

This new Hamiltonian is now of dimensions $N_2 \times N_2$, so it is smaller than the original matrix in the full basis and one could expect it would be easier to diagonalize. But the new matrix is now ε-dependent, so the eigenvalue equation becomes in fact a nonlinear one.

The idea is now to approximate this $H_{\text{eff}}(\varepsilon)$ by an ε-independent Hamiltonian $\tilde{H}_{\text{eff}}$. One defines a set of downfolded ε-dependent orbitals

$$\phi_a(\varepsilon) := \varphi_a + \varphi_b(\varepsilon\mathbb{1}^{(B)} - H^{(B)})^{-1} V^*_{ba} \tag{2.10}$$

where $\{\varphi\} = \{\varphi_1, \ldots, \varphi_{N_1}\}$ is the basis, in which the original (full) matrix H was written. a and b are the indices for the subspaces A and B respectively. Projection onto the B-orbitals yields:

$$\langle\varphi_b|H - \varepsilon|\phi_a(\varepsilon)\rangle = 0_{ba} \tag{2.11}$$

Projection onto the A-dimensions yields:

$$\langle\varphi_a|H - \varepsilon|\phi_a(\varepsilon)\rangle = \underbrace{H_{aa} + V_{ab}(\varepsilon\mathbb{1}^{(B)} - H^{(B)})^{-1} V^*_{ba}}_{H_{\text{eff}}} - \varepsilon\mathbb{1}_{aa} =: -G_{aa}(\varepsilon)^{-1} \tag{2.12}$$

One tries to find an ε-independent approximation χ_a to the set $\phi_a(\varepsilon)$. Therefore one forms the set of contracted Greens functions $\phi_a(\varepsilon)G_{aa}(\varepsilon)$ and adds an analytical function of ε, a matrix $P(\varepsilon)$, such that it coincides with the set $\chi_a^{(N)} G_{aa}(\varepsilon)$ when ε is on an energy mesh $[0 \ldots N]$:

$$\chi_a G_{aa}(\varepsilon) = \phi_a(\varepsilon)G_{aa}(\varepsilon) + P(\varepsilon), \text{ for } \varepsilon = [0 \ldots N] \tag{2.13}$$

Taking the so-called divided difference[1] $\frac{\Delta^N}{\Delta[0\ldots N]}$ on both sides yields

$$\chi_a \frac{\Delta^N G_{aa}}{\Delta[0\ldots N]} = \frac{\Delta^N \phi_a G_{aa}}{\Delta[0\ldots N]} \tag{2.14}$$

provided for $P(\varepsilon)$ a polynomial function of ε of $N-1$ degree is chosen, since then $\frac{\Delta^N P}{\Delta[0\ldots N]} = 0$ for any function of this class. So with

$$\chi_a^{(N)} = \frac{\Delta^N \phi_a G_{aa}}{\Delta[0\ldots N]} \left(\frac{\Delta^N G_{aa}}{\Delta[0\ldots N]} \right)^{-1} \tag{2.15}$$

one gets a set of (N_2) vectors in the reduced Hilbert space of dimension N_2, representing a set of orbitals, the so-called NMTOs, Muffin Tin Orbitals of order N. This NMTO set is not orthonormal in general. After orthonormalizing the set $\chi_a^{(N)}$, one obtains a new basis for the subspace of interest (A) and the original Hamiltonian H can be transformed into this basis yielding

$$\left(\tilde{H}_{\text{eff}}\right)_{aa'} = \chi_a^\dagger H \chi_{a'}. \tag{2.16}$$

So one ends up with an effective, energy-independent Hamiltonian of dimension $N_2 \times N_2$ which can now be diagonalized easier. The quality of this approximation depends in a very sensitive way on the choice of the energy-mesh points $\epsilon_\nu = \{\epsilon_0, \ldots, \epsilon_N\}$.

Thus, the presented downfolding method is able to create low-energy effective Hamiltonians, which is, in particular, very useful for correlated models in many-particle physics. Since here, problems become very complex due to the interactions, one is hardly interested in keeping the dimension of the Hilbert space as small as possible.

To realize this presented method numerically, we developed a program code with the use of the software Mathematica. We then applied it to different examples, which is presented in the following sections. Starting from a three-band model for the CuO_2-plane, we downfold to one band. This approach is presented in Sec. 2.2. Then we perform the downfolding from eight to three as well as from eight to one band, presented in Sec. 2.3.

[1] For a definition of the divided difference, see Ref. [5] p. 102.

2.2 The CuO_2 plane in $La_{2-x}Sr_xCuO_4$

One important parent compound for high-temperature superconducting materials is La_2CuO_4. The crystal structure of this material can be seen in Fig. 2.1. The typical property of all HTSC materials out of the class of the cuprates is the presence of two-dimensional planes, built up of copper and oxygen atoms, which appear periodically in the material. The characteristic properties of these materials are due to the dynamic of the electrons in these copper-oxide (CuO_2) planes, especially charge transport, which is responsible for the superconducting phase.

Therefore, the important physics takes place in these CuO_2-planes but is, of course, influenced by the region in between the planes. The effect of this region is to act as a charge reservoir for the planes. By replacing a few

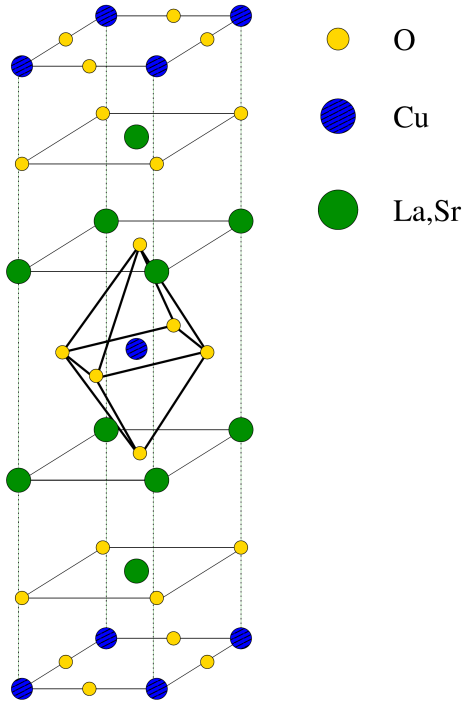

Figure 2.1: Crystal structure of $La_{2-x}Sr_xCuO_4$. In the middle of the elementary cell as well as at the top (and bottom) the CuO_2-planes can be seen, which are responsible for the charge transport in the superconducting phase

percent of the La atoms by Sr atoms one can actively control the number of conduction electrons in the planes. This is called a doped case and is symbolized by writing $La_{2-x}Sr_xCuO_4$, with the variable x quantifying the amount of La replaced by Sr atoms. Since Sr has one electron less than La in its outermost shell, the material gets additional charge carriers, or more exact the CuO_2-planes will become doped with holes. The electron configurations of the constituents of the compound are the following:

atom	number of electrons	atomic configuration	ionisation state in the crystal
La	57	$[Xe]6s^25d^1$	La^{3+}
Sr	38	$[Kr]5s^2$	Sr^{2+}
Cu	29	$[Ar]3d^{10}4s^1$	Cu^{2+}
O	8	$[He]2s^22p^4$	O^{2-}

In the crystal, the La atoms give away three electrons to get a full shell configuration with La^{3+}, the O atoms take two electrons to fill their $2p$-shell and get in the O^{2-} state. To assure the neutrality of the whole compound, the Cu atom has to loose two electrons to get into the Cu^{2+} state. It looses the $4s$ electron and one d electron, remaining at a $3d^9$ configuration. Since this means an unpaired electron in the d shell, the copper atom has a net spin of $1/2$. One also can say that there is a hole of spin $1/2$ on the Cu atom.

Due to the fact that the $Cu-d$ band is half filled, one should expect the system to be metallic. However, La_2CuO_4 is an insulator with a gap of about $2eV$. Experimentally La_2CuO_4 is an anti-ferromagnet, so that each $3d^9$ state has an unpaired spin aligned opposite to the spin of its neighbors. From spectroscopy one knows that in Cu the $3d^9$ state is lower by about $8eV$ than the $3d^8$ state. In the doped case of $La_{2-x}Sr_xCuO_4$ one sees from valence counting that a corresponding number of oxygen atoms will go from $O^{2-}(p^8)$ state to the $O^-(p^7)$ state, so the oxygen in the CuO_2-plane will become doped with holes. These holes hybridize strongly with the Cu states.

2.2.1 The model Hamiltonian

A simple model Hamiltonian which captures the physics discussed in the previous section, needs to include both the hybridization of the oxygen p and copper d orbitals, as well as the effect of strong correlations inhibiting

the formation of $3d^8$ state. One therefore needs a three-band tight-binding model Hamiltonian [8]. The orbitals considered in this three band model are the following (see Fig. 2.2):

- the $3d_{x^2-y^2}$-orbital of Cu
- the $2p_x$-orbital of $O1$ (oxygen atom located between two copper atoms in x-direction)
- the $2p_y$-orbital of $O2$ (oxygen atom located between two copper atoms in y-direction)

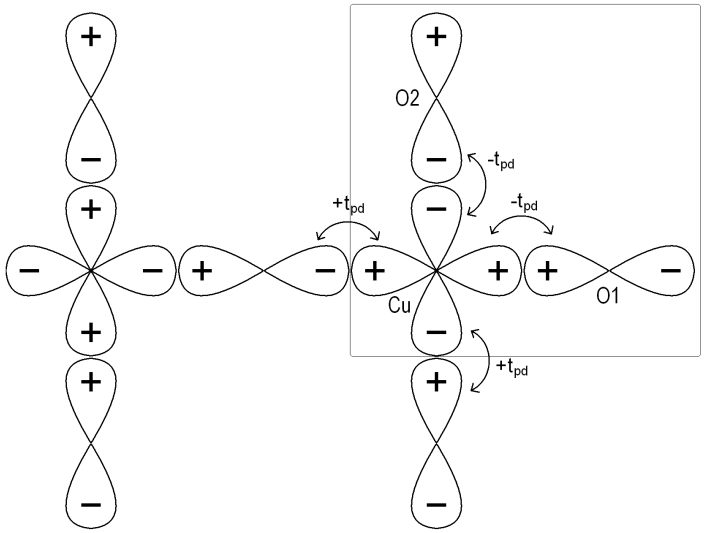

Figure 2.2: The CuO_2-plane of $La_{2-x}Sr_xCuO_4$: The $Cu - d_{x^2-y^2}$, $O1 - p_x$ and $O2 - p_y$ - orbitals and the hoppings between them. The sign of the hopping parameters t_{pd} depends on the bonding or antibonding overlap of the wavefuncions.

One can now define the corresponding tight-binding Hamiltonian:

$$H = H_0 + H_{dp} \tag{2.17}$$

with

$$H_0 = \sum_{i\sigma} \left(\epsilon_d^0 n_{d_{i\sigma}} + \epsilon_p^0 n_{p_{ix\sigma}} + \epsilon_p^0 n_{p_{iy\sigma}} \right) \tag{2.18}$$

$$\begin{aligned} H_{dp} = &- t_{pd} \sum_{i\sigma} \left(d_{i\sigma}^\dagger p_{ix\sigma} + d_{i\sigma}^\dagger p_{iy\sigma} + h.c. \right) \\ &+ t_{pd} \sum_{i\sigma} \left(d_{i\sigma}^\dagger p_{jx\sigma} + d_{i\sigma}^\dagger p_{j'y\sigma} + h.c. \right) \end{aligned} \tag{2.19}$$

Here, $d_{i\sigma}^\dagger$ ($d_{i\sigma}$) is the operator creating (annihilating) a hole with spin σ in the $d_{x^2-y^2}$-orbital of the copper atom at position R_i in the unit cell i. In analogy, $p_{ix\sigma}^\dagger$ ($p_{ix\sigma}$) and $p_{iy\sigma}^\dagger$ ($p_{iy\sigma}$) are the operators creating (annihilating) a hole with spin σ in the p_x-orbital of the oxygen atom O_1 and the p_y-orbital of the oxygen atom O_2 in the unit cell i. n denote the number operators for the corresponding orbital, defined e.g. as $n_{d_{i\sigma}} = d_{i\sigma}^\dagger d_{i\sigma}$. The indices j and j' denote the neighbor unit cells of the unit cell i, situated at R_i, in the $-x$ and $-y$ - directions respectively (see Fig. 2.3). The ϵ_d^0 and ϵ_p^0 are the on-site energies of the $Cu-d$ and $O-p$ orbitals. t_{pd} describe the amplitudes for hoppings of a hole between the neighboring $Cu-d$ and $O-p$ orbitals.

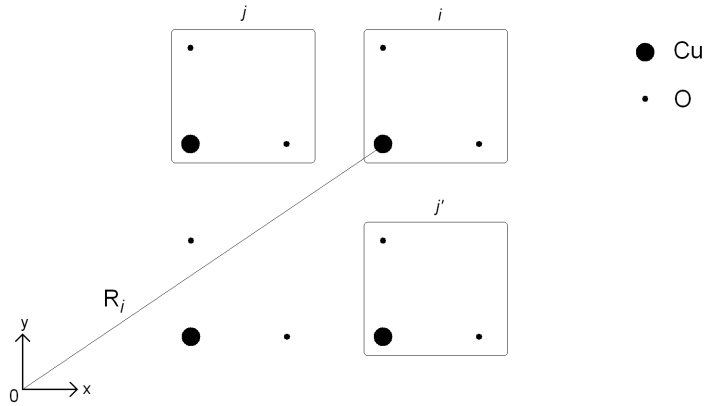

Figure 2.3: The CuO_2-plane of $La_{2-x}Sr_xCuO_4$: the elementary cell contains one copper and two oxygen atoms. The cell i is situated at R_i and has the neighbor cells j and j'.

The first line in (2.19) describes the hoppings between the orbitals in the unit cell i, the second line those between orbitals belonging to different

(neighbored) unit cells. In the latter case the sign of the overlapping wavefunctions is different, so we get an additional minus sign which leads to a positive sign for the t_{pd}. See Fig. 2.2 for details.

The solution of the tight binding hamiltonian leads to two hybridized $Cu-O$ bands and one non-hybridized oxygen level. In a real three dimensional crystal the non-hybridized level will couple to atoms from other planes and move down to lower energies, so we do not consider it further.

In order to calculate the band structure, the Fourier representations are introduced:

$$d_{i\sigma} = \frac{1}{\sqrt{N}} \sum_k e^{i\vec{k}\vec{R}} d_{k\sigma} \tag{2.20}$$

$$p_{ix\sigma} = \frac{1}{\sqrt{N}} \sum_k e^{i\vec{k}(\vec{R}_i + \frac{a}{2}\vec{e}_x)} p_{kx\sigma} \tag{2.21}$$

$$p_{iy\sigma} = \frac{1}{\sqrt{N}} \sum_k e^{i\vec{k}(\vec{R}_i + \frac{b}{2}\vec{e}_y)} p_{ky\sigma} \tag{2.22}$$

Then, with the field operator

$$\Psi^\dagger_{k\nu\sigma} = \left(d_{k\sigma}, p^\dagger_{kx\sigma}, p^\dagger_{ky\sigma} \right) \tag{2.23}$$

one can write the quadratic part of the Hamiltonian $H = H_0 + H_{dp}$:

$$H = \sum_{k\nu\nu'\sigma} \Psi^\dagger_{k\nu\sigma} H_{k\nu\nu'} \Psi_{k\nu'\sigma} \tag{2.24}$$

Thus, the Hamiltonian matrix can be written as

$$H_{k\nu\nu'} = \begin{pmatrix} \epsilon_d^0 & 2it_{pd} \sin\frac{a}{2}k_x & 2it_{pd} \sin\frac{b}{2}k_y \\ -2it_{pd} \sin\frac{a}{2}k_x & \epsilon_p^0 & 0 \\ -2it_{pd} \sin\frac{b}{2}k_y & 0 & \epsilon_p^0 \end{pmatrix} \tag{2.25}$$

2.2.2 Downfolding results

We now want to replace the three orbitals in the unit cell, the $Cu - d_{x^2-y^2}$, $O1 - p_x$ and $O2 - p_z$ orbitals by just one orbital at the Cu site. The oxygen-p orbitals are not simply removed, but are downfolded into this new $Cu - d_{x^2-y^2}$-orbital. We therefore apply the downfolding procedure as described in section 2.1 to the three-band Hamiltonian $H_{k\nu\nu'}$ in Eq. (2.25). We downfold

to the first dimension, i.e. the one for the $Cu{-}d_{x^2-y^2}$-band. For the numerical calculation we take the following values: $a = b = 1$, $\epsilon_d^0 = 0$, $\epsilon_p^0 = 3$ and $t_{pd} = 1$. A plot of the original band structure of the three band Hamiltonian together with the downfolded band is shown in Fig. 2.4. For the chosen energy-points $\epsilon_\nu = \{-0.5, -1.5\}$ we observe a good agreement.

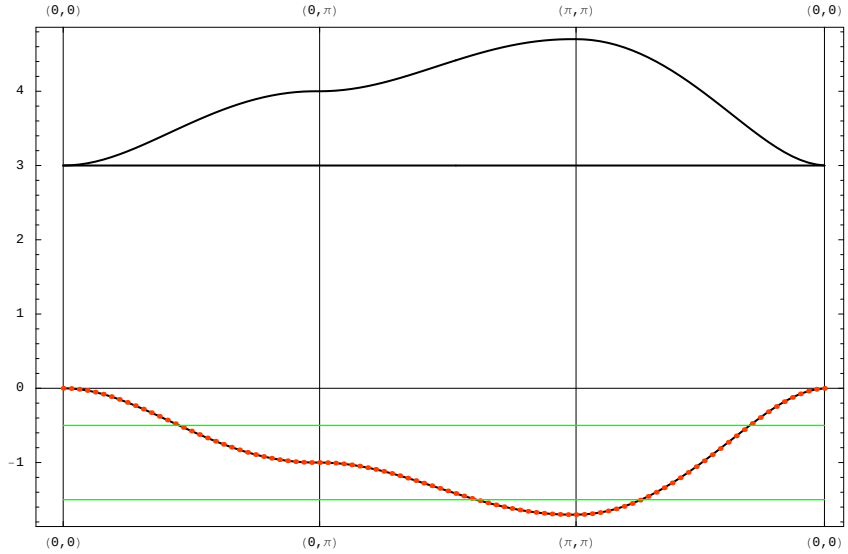

Figure 2.4: The band structure for the CuO_2-plane of $La_{2-x}Sr_xCuO_4$ (black) and the downfolding to the $Cu{-}d_{x^2-y^2}$-band (dotted red) with the chosen ϵ_ν-points (green). The energy scale is relative to ϵ_d^0.

As already mentioned above, the quality of the downfolding method, i.e. the agreement of the downfolded band to the exact one, depends strongly on the position and the number of the ϵ_ν-points chosen for the energy mesh in Eq. (2.14).

In order to have a measure of the quality of the approximation, we introduce an error E defined by

$$E = \sqrt{\sum_k \left(\varepsilon_{df}(k) - \varepsilon_{ex}(k)\right)^2}, \tag{2.26}$$

which is a suitable quantity for the deviation between the downfolded band $\varepsilon_{df}(k)$ and the exact band $\varepsilon_{ex}(k)$ in k-space. This error is computed for each calculation and compared.

We now investigate the accuracy of the downfolding approach depending on the choice of the energy mesh $\epsilon_\nu = \{\epsilon_0, \ldots, \epsilon_N\}$. We carry out calculations for three different energy meshes, containing one, two, and three energy points ϵ_ν defined in the following way (see Fig. 2.5):

$$\epsilon_\nu^{(1)} = \{\epsilon\} \qquad \text{(green)}$$
$$\epsilon_\nu^{(2)} = \{\epsilon - \delta^{(2)}, \epsilon + \delta^{(2)}\} \qquad \text{(red)}$$
$$\epsilon_\nu^{(3)} = \{\epsilon - \delta^{(3)}, \epsilon, \epsilon + \delta^{(3)}\} \qquad \text{(blue)}$$

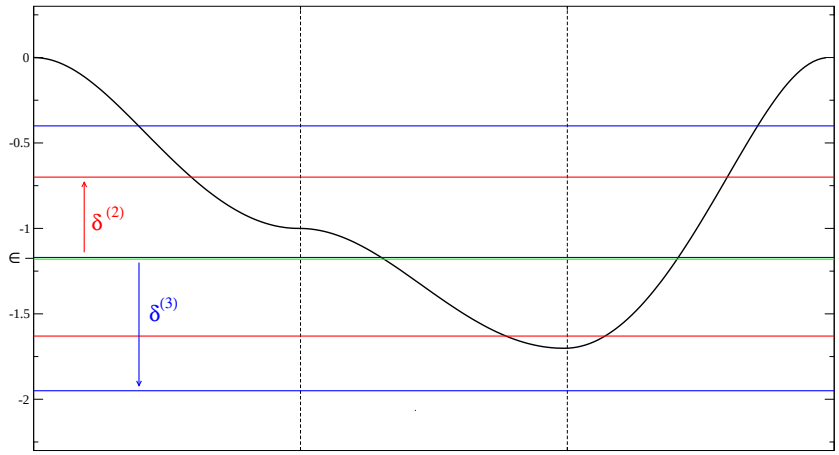

Figure 2.5: The energy mesh points used for the downfolding of $La_{2-x}Sr_xCuO_4$: the unrenormalized $Cu - d_{x^2-y^2}$-band in black and the one-point mesh in green, the two point mesh in red and the three-point mesh in blue, each at the optimal position (see Fig. 2.6).

First, we do the calculations for the one-point mesh $\epsilon_\nu^{(1)}$, depending on ϵ. We find a minimal error $E = 0.007$ for a value of $\epsilon = -1.17$. For the following calculations, the two and three-point mesh $\epsilon_\nu^{(2)}$ and $\epsilon_\nu^{(3)}$ take this value as their center. For each mesh we investigate the dependence of the error E on the spacing-parameter δ. The results are shown in Fig. 2.6. From $\delta = 0$, where of course all the three meshes condense to the one-point mesh, we observe for increasing δ a decreasing error until we reach a minimum, before it increases again very strongly. For the two-point mesh the minimal error is found for an optimal spacing at $\delta_{min}^{(2)} \approx 0.5$ and for the three-point mesh at $\delta_{min}^{(2)} \approx 0.8$. The illustration in Fig. 2.5 corresponds to this situation.

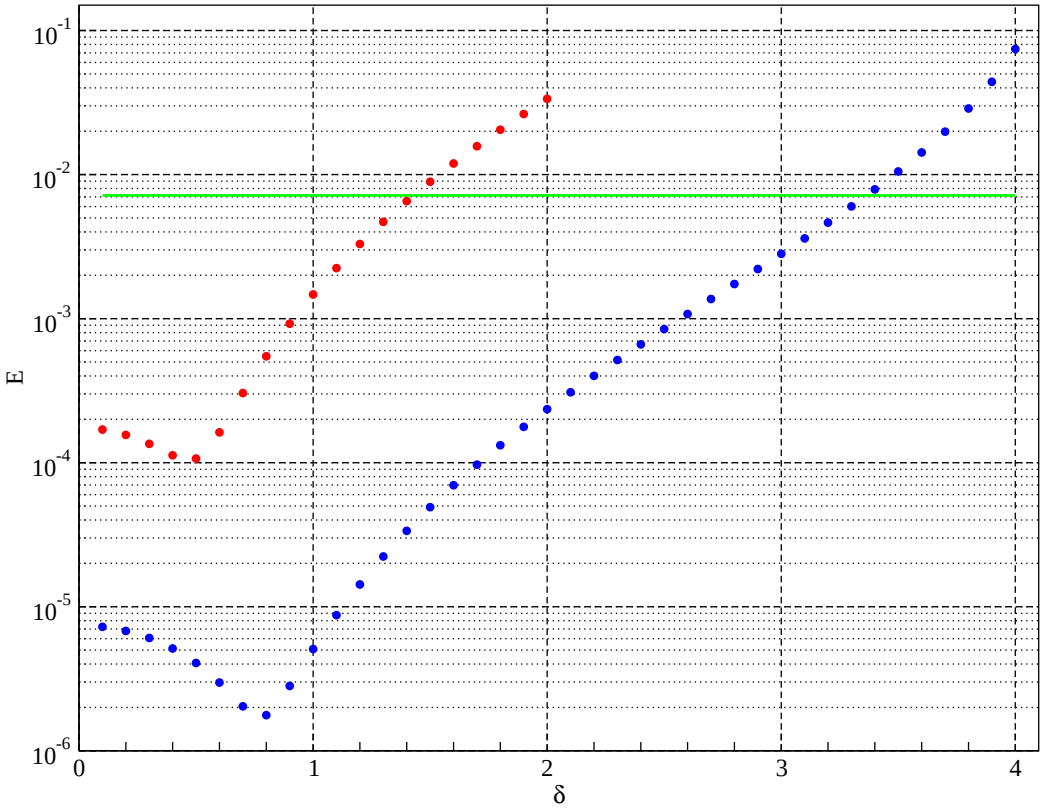

Figure 2.6: The Error E of the downfolded $Cu - d_{x^2-y^2}$-band in dependence of the distance δ between the mesh-points for one (green), two (red) and three points (blue). (see Fig. 2.5)

In the region of optimal spacing δ, we observe a decrease of the error between one and two orders of magnitude for each additional energy point. However, due to the strong dependence on δ, it cannot be generally stated, that increasing the number of energy points leads automatically to a reduction of the error. We see that for large δ, i.e. for mesh-points far away from the searched band, the error for taking more points is even bigger than for just one point. But, of course, this one single point is chosen at its optimal position, which in general, we don't know in advance. Therefore, adding more points will reduce the error, as long as their spacing is not too big (compared to the bandwidth of the downfolded band), that means the mesh becomes more dense. In practice, the number of points is limited by the computation time.

Another interesting question is how the accuracy of the downfolding procedure depends on the orbital separation energy $\Delta = \epsilon_d^0 - \epsilon_p^0$ between the $Cu - d_{x^2-y^2}$ and $O - p$ orbitals. Fig. 2.7 shows the error of the downfolded band in dependence of Δ. Since Δ changes the bandwidth W of the band (the bandwidth decreases with increasing Δ), the error must be taken relative to the bandwidth to produce a meaningful plot.

We consider a mesh of three energy points, $\epsilon_\nu = \{\epsilon_1, \epsilon_2, \epsilon_3\}$ with the

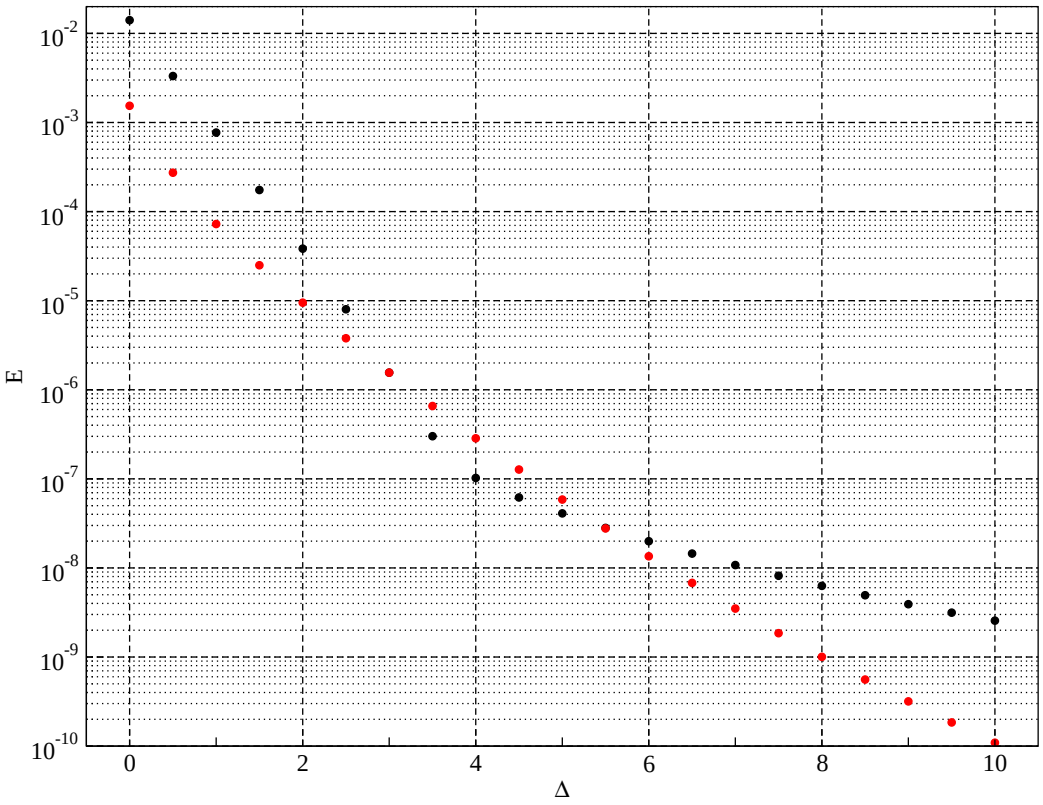

Figure 2.7: The Error E of the downfolded $Cu - d_{x^2-y^2}$-band relative to the bandwidth in dependence of the orbital separation Δ to the $O - p$-orbitals. For a 3-point mesh at fixed position (black) and at Δ-dynamical positions (point distance δ depending on the bandwidth) (red).

following values

$$\epsilon_1 = \epsilon_d^0 - \frac{1}{4}W$$
$$\epsilon_2 = \epsilon_d^0 - \frac{1}{2}W$$
$$\epsilon_3 = \epsilon_d^0 - \frac{3}{4}W$$

in which the value of W is obtained in two different ways: In a first calculation (black), a fixed mesh with $W(\Delta = 3)$ is used for all Δ. In a second calculation (red), the mesh is set to Δ-dynamical positions at $W(\Delta)$, so the mesh-points change for every calculation.

Since the bandwidth W chances with Δ, the latter method is of course more efficient than the first case, which is plotted in comparison in Fig. 2.7. As we would expect, it shows in general a bigger error, except in the interval from $\Delta = 3$ to about 5.5. This is due to the fact, that the chosen position of the mesh points (at 1/4, 1/2, 3/4 of the bandwidth) is obviously not the optimal one.

Generally we observe an exponential decrease of the relative error with the band separation energy Δ. This result we would expect, since increasing Δ means that the overlap of the orbitals becomes smaller, i.e. a relative decrease of the non-diagonal elements in the Hamilton matrix H (Eq. 2.25), to which we apply the downfolding (see Eq. 2.9).

To conclude, it can be said that the choice of the position and the number of energy-mesh points ϵ_ν is of significant importance for the accuracy of the downfolded band with respect to the original one. The points have to lie in the region of the downfolded band, and an increasing number will increase the accuracy, as long as they have 'reasonable' spacing and positions with respect to the bandwidth.

2.3 The bilayer CuO_2 planes in $YBa_2Cu_3O_7$ cuprate

Another important HTSC material out of the class of the cuprates is $YBa_2Cu_3O_7$. This compound is, concerning the CuO_2-planes, very similar to $La_{2-x}Sr_xCuO_4$ described in section 2.2. Its crystal structure is shown in Fig. 2.8. The region of interest is again the CuO_2 planes. Due to the crystal structure of $YBa_2Cu_3O_7$, i.e. the difference between Y and Ba atoms, these planes are not completely flat, but are dimpled, which means that the oxygen atoms are slightly out of plane. This is an important property of this material. Due to this fact, the two CuO_2 planes are not identical any more and cannot be described independently. Thus, in contrast to the previously described $La_{2-x}Sr_xCuO_4$, this material forms a bilayer, consisting of two CuO2 planes around the Yttrium atom. Since there are two possibilities to combine the wavefunctions of the two single planes, we have to consider two types of wavefunctions, the even and odd ones, for the bilayer.

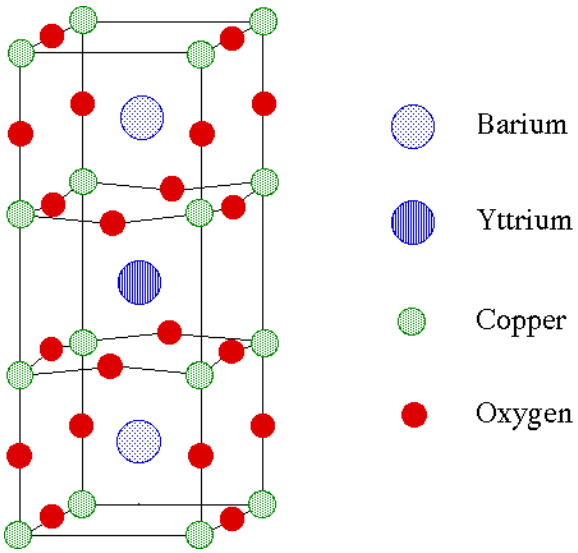

Figure 2.8: The crystal structure of $YBa_2Cu_3O_7$. Above and below the Yttrium atom in the center, the dimpled CuO_2-planes, which form the bilayer, can be seen.

2.3.1 The model Hamiltonian

By downfolding from the full LDA multi-band Hamiltonian, Andersen et al. [9, 3] derived an eight-band, tight-binding Hamiltonian, H_8, for the CuO_2 bilayer. The remaining orbitals are $Cu - d_{x^2-y^2}$, $Cu - s$, $O1 - p_x$, $O2 - p_y$, $O1 - p_z$, $O2 - p_z$, $Cu - d_{xz}$, $Cu - d_{yz}$ and are shown in Fig. 2.9. Four of these eight orbitals have σ character and four have π character. According to Ref. [3], is "the reason for keeping in the Hamiltonian particularly those eight orbitals, that these orbitals are the ones which after orthogonalization describe the LDA plane-bands accurately over a $\pm 1eV$ range with nearest neighbor hoppings only, that is, with the minimal number of parameters. The eight-band Hamiltonian is thus the one which is 'chemically' meaningful and sufficiently simple" for further treatments.

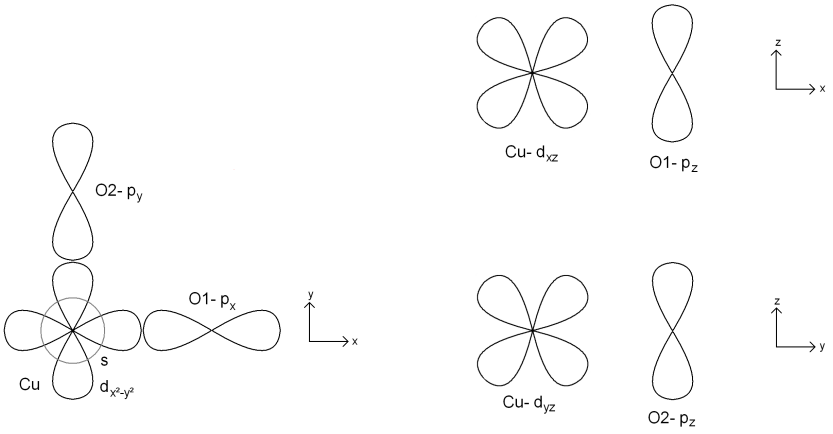

Figure 2.9: The copper-oxide plane of $YBa_2Cu_3O_7$: the considered orbitals forming σ -bonds (left) and those forming π -bonds (right).

The Hamiltonian matrix is written in the following form:

$$H_8 = \begin{pmatrix} H_\sigma & H_{\sigma\pi} \\ H_{\pi\sigma} & H_\pi \end{pmatrix} \tag{2.27}$$

with H_σ, the Hamiltonian restricted to the σ-bonding orbitals $|Cu - d_{x^2-y^2}\rangle$,

$|Cu-s\rangle$, $|O1-p_x\rangle$, $|O2-p_y\rangle$:

$$H_\sigma = \begin{pmatrix} \epsilon_d & 0 & 2t_{xd}\sin\frac{a}{2}k_x & -2t_{yd}\sin\frac{b}{2}k_y \\ 0 & \epsilon_s & 2t_{sx}\sin\frac{a}{2}k_x & 2t_{sy}\sin\frac{b}{2}k_y \\ 2t_{xd}\sin\frac{a}{2}k_x & 2t_{sx}\sin\frac{a}{2}k_x & \epsilon_p & 0 \\ -2t_{yd}\sin\frac{b}{2}k_y & 2t_{sy}\sin\frac{b}{2}k_y & 0 & \epsilon_p \end{pmatrix} \tag{2.28}$$

and H_π restricted to the π-bonding orbitals $|O1-p_z\rangle$, $|O2-p_z\rangle$, $|Cu-d_{xz}\rangle$, $|Cu-d_{yz}\rangle$:

$$H_\pi = \begin{pmatrix} \epsilon_{za} & -4t_{zz}\cos\frac{a}{2}k_x\cos\frac{b}{2}k_y & 2t_{z,xz}\sin\frac{a}{2}k_x & 0 \\ -4t_{zz}\cos\frac{a}{2}k_x\cos\frac{b}{2}k_y & \epsilon_{zb} & 0 & 2t_{z,yz}\sin\frac{b}{2}k_y \\ 2t_{z,xz}\sin\frac{a}{2}k_x & 0 & \epsilon_{xz} & 0 \\ 0 & 2t_{z,yz}\sin\frac{b}{2}k_y & 0 & \epsilon_{yz} \end{pmatrix} \tag{2.29}$$

Finally,

$$H_{\sigma\pi} = H_{\pi\sigma}^T = \begin{pmatrix} 2t_a\sin\frac{a}{2}k_x & -2t_b\sin\frac{b}{2}k_y & 0 & 0 \\ 0 & 0 & 0 & 0 \\ 0 & 0 & 0 & 0 \\ 0 & 0 & 0 & 0 \end{pmatrix} \tag{2.30}$$

is the block mixing the σ- and π-orbitals.

Here, a and b are the lattice parameters in x and y direction of the plane, the ϵ's denote the on-site energies for the corresponding orbitals. For the indices the following abbreviations are used: d for the $Cu-d_{x^2-y^2}$ orbital, s for $Cu-s$, x for $O1-p_x$, y for $O2-p_y$, za for $O1-p_z$, zb for $O2-p_z$, xz for $Cu-d_{xz}$, yz for $Cu-d_{yz}$.For the odd (o) and the even (e) plane the numerical values, given in meV, are the following:

meV	ϵ_d	ϵ_s	ϵ_x	ϵ_y	$\epsilon_{za}=\epsilon_{zb}$	$\epsilon_{xz}=\epsilon_{yz}$
o	-2308	$+4844$	-3199	-3082	-1602	-3639
e	-2402	$+3378$	-3476	-3267	-2304	-3056

The t's denote the hopping parameters in between the eight considered orbitals for nearest-neighbor sites, the meaning of the indices is in analogy to above. The only case where second-nearest neighbor hopping is considered, is the hopping between $O1-p_z$, and $O2-p_z$ with the parameter t_{zz}. t_a and t_b describe the hopping between the $Cu-d_{x^2-y^2}$ orbital and the oxygen p_z orbitals (on the a and b axis respectively). This hybridisation of σ and π

bonds is a result of the dimpling of the CuO_2 plane. The hopping parameter depends on the dimpling angle α, which is about 7°, with the relation $t_a, t_b \propto \sin\alpha$. The numerical values for the hopping parameters are the following:

meV	t_{xd}	t_{yd}	t_{sx}	t_{sy}	t_{zz}	$t_{z,xz}$	$t_{z,yz}$	t_a	t_b
o	1576	1556	2024	2006	120	829	831	228	223
e	1599	1588	2582	2517	12	543	524	267	249

2.3.2 Downfolding Results

Downfolding to three bands

In this section, we show how the downfolding procedure of section 2.1 is applied to the eight-band Hamiltonian H_8 discussed above. The aim is to have a single orbital per atomic site to describe the physics in the plane. Since the σ-orbitals cause the strongest hybridisations, i.e. have the biggest hopping parameters, we downfold to the corresponding three orbitals: $Cu - d_{x^2-y^2}$, $O1 - p_x$, $O2 - p_y$. The fact, that we choose the $Cu - d$ and not the $Cu - s$ orbital is due to the fact that the $Cu - s$ band lies at too high energy. In Fig. 2.10 the projections of those three orbitals to the eight orbitals are shown.

As energy-mesh we take two points at $\epsilon_1 = -5$ and $\epsilon_2 = 5$ relative to ϵ_d. This covers the energy range where the bands of interest are situated. The result of the downfolding is shown in Fig. 2.11. Even for just two ϵ-points we observe a rather good agreement with the bands obtained from full diagonalisation of H_8. The big deviations near the Γ-point at $k = (0, 0)$ especially for the $Cu - d_{x^2-y^2}$-band are explained by the strongly mixed character of the bands in this region and is something we would have expected.

Downfolding to one band

A further step is to keep in the final model just one orbital per CuO_2-unit cell, i.e. one orbital around the copper site, where all the others are folded into. We therefore downfold the eight-band Hamiltonian H_8 to the single $Cu - d_{x^2-y^2}$ band.

The result is plotted in Fig. 2.12 together with the original bands of H_8. Again we observe a rather good agreement with the $Cu - d_{x^2-y^2}$ band obtained from full diagonalisation. As energy-mesh we take here two points at $\epsilon_1 = 1.5$ and $\epsilon_2 = 3eV$ above ϵ_d. This is within the energy range of the

concerned band. For a good result, it is important to choose no energy-mesh point in the energy region of another band, which has some (not negligible) $Cu - d_{x^2-y^2}$ character.

This reduced one-band model contains not only hoppings between nearest-neighbor orbitals, but also longer range hoppings. These can be obtained by observing that the Fourier transformation of the one-band Hubbard model is given by:

$$\begin{aligned} H_1(k) =& \epsilon - 2t(\cos ak_x + \cos bk_y) + 4t' \cos ak_x \cos bk_y - 2t''(\cos 2ak_x + \cos 2bk_y) \\ &+ 4t^{(3)}(\cos ak_x \cos 2bk_y + \cos 2ak_x \cos bk_y) + 4t^{(4)} \cos 2ak_x \cos 2bk_y \\ &- 2t^{(5)} (\cos 3ak_x + \cos 3bk_y) + \dots \end{aligned} \tag{2.31}$$

in terms of the hopping parameters $t^{(n)}$ for the $(n+1)$-nearest neighbor. By fitting with Eq. (2.31) the band obtained by downfolding, we obtain the following numerical values for the hopping parameters up to the 6^{th} nearest neighbor for the odd (o) and even (e) bilayer:

meV	t	t'	t''	$t^{(3)}$	$t^{(4)}$	$t^{(5)}$
o	348	102	59	16	0.07	9.1
e	420	121	111	20	5.8	33

This is in very good agreement with the result obtained for the exact diagonalized band by Andersen et al. [3]:

meV	t	t'	t''	$t^{(3)}$	$t^{(4)}$	$t^{(5)}$
o	349	96	62	18	1	10
e	422	113	110	20	5	32

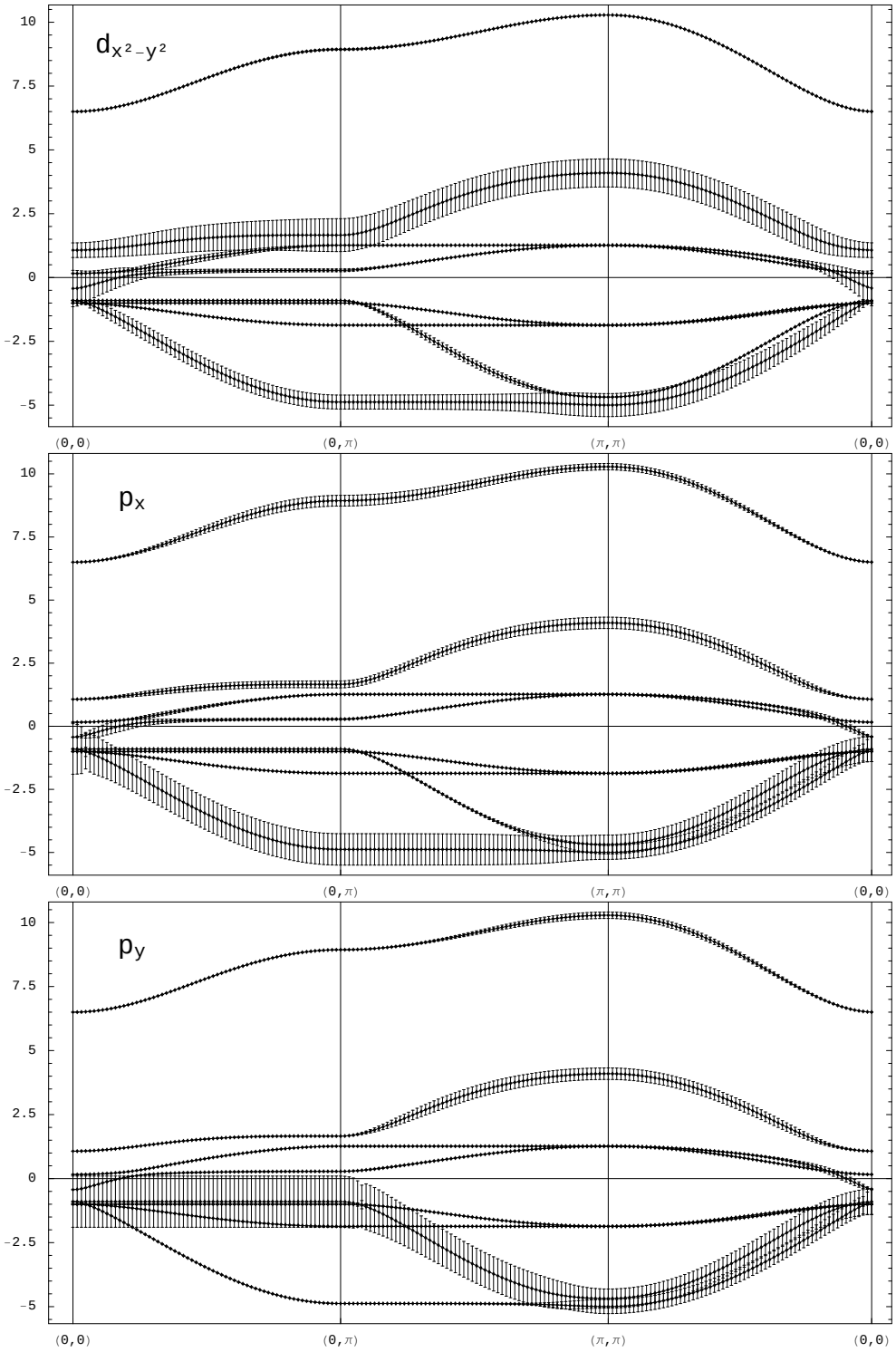

Figure 2.10: Band structure of $YBa_2Cu_3O_7$ obtained by diagonalizing H_8, together with the weights of the projections to the $Cu-d_{x^2-y^2}$, $O1-p_x$ and $O2-p_y$ orbitals. The energy scale is relative to ϵ_d.

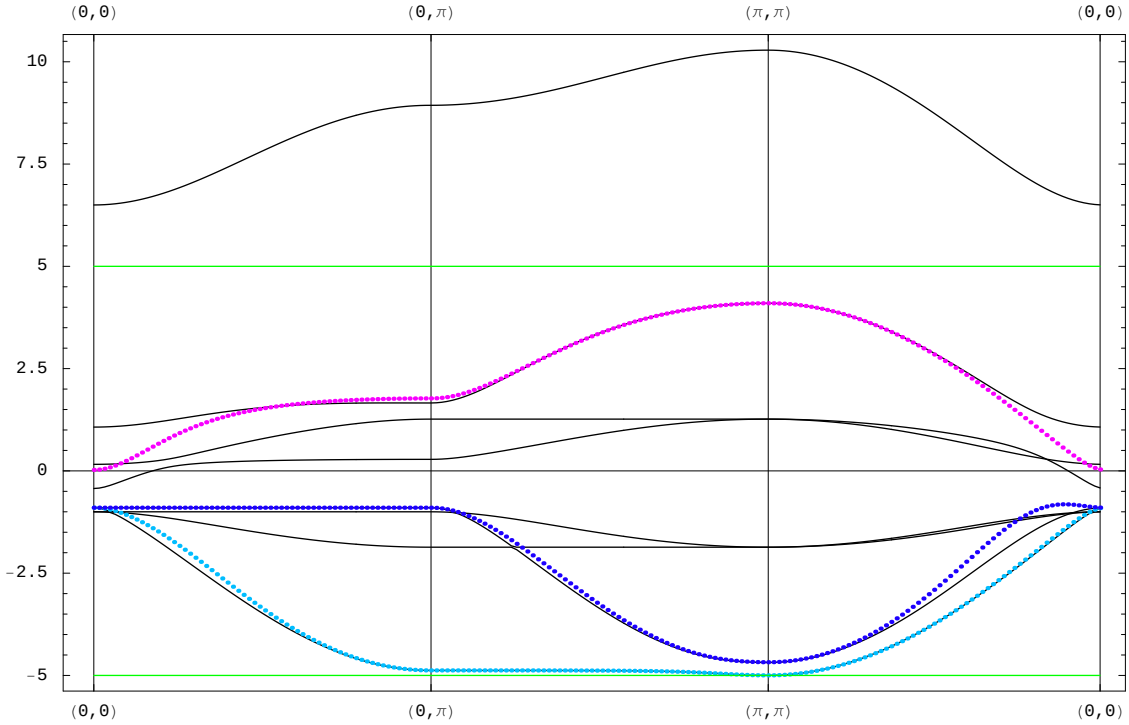

Figure 2.11: Downfolding to three bands for $YBa_2Cu_3O_7$: comparison of the exact bands (black) of H_8 and the downfolded bands (dotted in color) for $Cu - d_{x^2-y^2}$, $O1-p_x$ and $O2-p_y$. The green lines correspond to the energy-mesh points used for the downfolding. The energy scale is relative to ϵ_d.

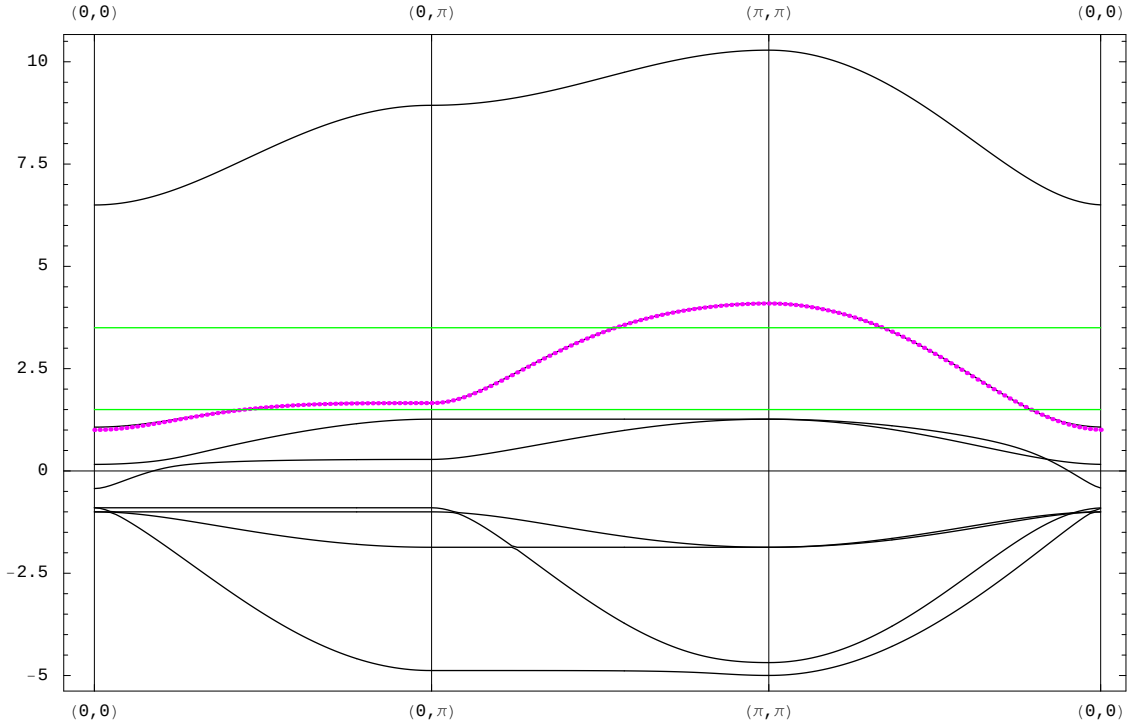

Figure 2.12: Downfolding to one band for $YBa_2Cu_3O_7$: comparison of the exact bands (black) of H_8 and the downfolded band (dotted in color) for $Cu - d_{x^2-y^2}$. The green lines correspond to the energy-mesh points used for the downfolding. The energy scale is relative to ϵ_d.

Chapter 3

The interacting Hubbard model

In the previous chapter the non-interacting low-energy Hamiltonian (a tight-binding model) was described. The results of these calculations are now used to construct an extended model Hamiltonian, where to the tight-binding model (which considers hoppings) an interaction term is added, which takes into account the Coulomb interaction between the electrons. This is called the Hubbard model [10, 11] and is introduced in the first section of this chapter. In the following sections, different levels of approximations are discussed. Starting from a local picture in the limit of isolated atoms, i.e. the atomic limit, the so-called Hubbard-I approximation [10] is derived. Then, the Cluster perturbation theory (CPT)[12] is presented as an improvement of the latter method. Finally, an extension of CPT is introduced, the Variational Cluster Approach (VCA) [13, 14, 15, 16, 17, 18, 19], which requires self-consistent calculations. The latter method is then applied in chapter 4 to analyze the electronic properties of $SrVO_3$.

3.1 Hubbard model and different approximations

Many of the most interesting properties of materials such as magnetic ordering or superconductivity require theories that go beyond the independent electron approximation. In order to understand the physical phenomena it is necessary to take into account electron correlations. The simplest model of correlated electrons is the Hubbard model [10, 11, 20] which has to be formulated in terms of localized orbitals, e.g. in terms of Wannier functions.

This section follows mainly the presentation in the book of F.Gebhard [20].

In the one-band Hubbard model there is one electron orbital per unit cell. It is assumed that one can restrict to only one valence orbital per atom. Obviously each orbital can accommodate 0, 1, or 2 electrons. The hamiltonian consists of a kinetic energy term describing the hopping amplitude, denoted by t, and an interaction term describing the on-site Coulomb repulsion, denoted by U. In second quantized form, the Hubbard Hamiltonian can, thus, be written:

$$H_{\text{Hubbard}} = \sum_{R_i,\sigma}(\epsilon_0 - \mu)n_{R_i\sigma} - t\sum_{R_i,R_j,\sigma} c^{\dagger}_{R_i\sigma}c_{R_j\sigma} + U\sum_{R_i} n_{R_i\uparrow}n_{R_i\downarrow} \tag{3.1}$$

where $n_{R\sigma} = c^{\dagger}_{R\sigma}c_{R\sigma}$ with $c^{\dagger}_{R\sigma}$ ($c_{R\sigma}$) creating (annihilating) an electron with spin σ at position R. The first term considers the on-site energy ϵ_0 and the chemical potential μ.

The model is first studied for the atomic limit (t=0) [10] and then solved within the Hubbard-I approximation[10, 20].

3.1.1 Atomic limit

One limit case of the one band Hubbard model is, when the hopping parameters t are set to zero. This means that electrons cannot move between different atomic sites, so each atom is isolated from the others. Thus, this case is called the atomic limit. The Hubbard Hamiltonian then reads:

$$H_{(t=0)} = \sum_{\sigma}(\epsilon_0 - \mu)n_{R\sigma} + \frac{U}{2}\sum_{\sigma} n_{R\sigma}n_{R-\sigma} \tag{3.2}$$

The one-particle retarded Green's function is defined as

$$G^{ret}_{\sigma}(R_1, R_2, t) = \Theta(t)\left\langle\left[c_{R_1\sigma}(t), c^{\dagger}_{R_2\sigma}\right]_+\right\rangle \tag{3.3}$$

with $[A,B]_- = AB - BA$ and $[A,B]_+ = AB + BA$ denoting the commutator and anticommutator of the operators A and B, respectively. Its Fourier transformation is denoted as $\left\langle\left\langle c_{R_1\sigma}; c^{\dagger}_{R_2\sigma}\right\rangle\right\rangle_{\omega}$.

In order to calculate the Green's function, the equation of motion theory is applied. One gets

$$\omega \left\langle\left\langle c_{R_1\sigma}; c^\dagger_{R_2\sigma}\right\rangle\right\rangle_\omega = \left\langle\left[c_{R_1\sigma}(t), c^\dagger_{R_2\sigma}\right]_+\right\rangle + \left\langle\left\langle [c_{R_1\sigma}, H]_- ; c^\dagger_{R_2\sigma}\right\rangle\right\rangle_\omega \tag{3.4}$$

One inserts the $t = 0$ Hubbard Hamiltonian (Eq. 3.2) in the commutator and after some computation one obtains

$$[c_{R_1\sigma}, H]_- = (\epsilon_0 - \mu)\, c_{R_1\sigma} + U c_{R_1\sigma} n_{R_1-\sigma} \tag{3.5}$$

So equation 3.4 becomes

$$\omega G_{R_1R_2\sigma}(\omega) = 1 + (\epsilon_0 - \mu)\, G_{R_1R_2\sigma}(\omega) + U\Gamma_{R_1R_2\sigma}(\omega) \tag{3.6}$$

Here the higher order two particle Green's function $\Gamma(\omega)$ has been defined.

$$\Gamma_{R_1R_2\sigma}(\omega) = \left\langle\left\langle c_{R_1\sigma} n_{-\sigma}; c^\dagger_{R_2\sigma}\right\rangle\right\rangle_\omega \tag{3.7}$$

For this Green's function one now calculates again the equation of motion:

$$\begin{aligned}
\omega\Gamma_{R_1R_2\sigma}(\omega) &= \left\langle\left[c_{R_1\sigma} n_{R_1-\sigma}, c^\dagger_{R_2\sigma}\right]_+\right\rangle + \left\langle\left\langle [c_{R_1\sigma} n_{R_1-\sigma}, H]_- ; c^\dagger_{R_2\sigma}\right\rangle\right\rangle_\omega \\
&= \delta_{R_1R_2}\langle n_{R_1-\sigma}\rangle + (\epsilon_0 - \mu)\left\langle\left\langle c_{R_1\sigma} n_{R_1-\sigma}; c^\dagger_{R_2\sigma}\right\rangle\right\rangle_\omega \\
&\quad + U\left\langle\left\langle c_{R_1\sigma} n^2_{R_1-\sigma}; c^\dagger_{R_2\sigma}\right\rangle\right\rangle_\omega \\
&= \delta_{R_1R_2}\langle n_{R_1-\sigma}\rangle + (\epsilon_0 - \mu + U)\,\Gamma_{R_1R_2\sigma}(\omega)
\end{aligned} \tag{3.8}$$

thus one gets the result for the two particle Green's function:

$$\Gamma_{R_1R_2\sigma}(\omega) = \frac{\delta_{R_1R_2}\langle n_{R_1-\sigma}\rangle}{\omega + \mu - \epsilon_0 - U} \tag{3.9}$$

inserting this result in the upper expression 3.6 one obtains

$$\omega G_{R_1R_2\sigma}(\omega) = 1 + (\epsilon_0 - \mu)\, G_{R_1R_2\sigma}(\omega) + U\frac{\delta_{R_1R_2}\langle n_{-\sigma}\rangle}{\omega + \mu - \epsilon_0 - U} \tag{3.10}$$

and so the resulting one-particle Green's function for the same site R is:

$$G_{RR\sigma}(\omega) = \frac{1 - \langle n_{R-\sigma}\rangle}{\omega + \mu - \epsilon_0} + \frac{\langle n_{R-\sigma}\rangle}{\omega + \mu - \epsilon_0 - U} \tag{3.11}$$

From this result one can easily see that the poles of the Green's function lie for ω at $\epsilon_0 - \mu$ and $\epsilon_0 - \mu + U$. So the density of states consists of two delta-peaks with energy distance U from each other. The electronic states are just allowed for these two energy values. This describes the two possible energies required to add a particle, $\epsilon_0 - \mu$ and $\epsilon_0 - \mu + U$ for single and double occupation respectively.

3.1.2 Hubbard-I approximation

Another limiting case apart from the atomic limit is the non-interacting limit, i.e. there is no interaction U in the Hubbard model ($U = 0$). In this case one has the very simple non-interacting Green's function

$$G^{(0)}(\omega) = \frac{1}{\omega + \mu - t} \tag{3.12}$$

Our goal is to solve the full model which includes interaction and hoppings, i.e. U and t, to describe the physics of our problem properly. Since the solution of the full Hubbard model is impossible, we have to look for approximations. Therefore the above two limits will be used in combination.

The following, so called Dyson, equation provides a relation between the Green's function of the full problem and the non-interacting Green's function:

$$G(\omega) = G^{(0)}(\omega) + G^{(0)}(\omega)\,\Sigma(\omega)\,G(\omega) \tag{3.13}$$

with the unknown self energy $\Sigma(\omega)$. The main idea of the so called Hubbard-I approximation [10, 20] is to replace this unknown quantity Σ by the self energy of the atomic limit

$$\Sigma(\omega) = \Sigma_{atomic}(\omega) \tag{3.14}$$

By using the results of the previous section, i.e. Eq. (3.11) the atomic self energy is calculated:

$$\begin{aligned}
\Sigma_{atomic}(\omega) &= G^{(0)}_{atomic}(\omega)^{-1} - G_{atomic}(\omega)^{-1} && (3.15)\\
&= (\omega + \mu - \epsilon_0) - \left(\frac{1 - \langle n_{-\sigma} \rangle}{\omega + \mu - \epsilon_0} + \frac{\langle n_{-\sigma} \rangle}{\omega + \mu - \epsilon_0 - U} \right)^{-1} \\
&= U \langle n_{-\sigma} \rangle + \frac{U^2 \langle n_{-\sigma} \rangle (1 - \langle n_{-\sigma} \rangle)}{\omega + \mu - \epsilon_0 - U(1 - \langle n_{-\sigma} \rangle)} && (3.16)
\end{aligned}$$

This leads to the resulting Green's function

$$G_k(\omega) = \frac{\omega + \mu - U(1 - \langle n_{-\sigma}\rangle)}{(\omega + \mu)(\omega + \mu - U) - \epsilon(k)(\omega + \mu - U(1 - \langle n_{-\sigma}\rangle))} \tag{3.17}$$

which can also be written in the form

$$G_k(\omega) = \frac{\alpha_1(k)}{\omega - \omega_1(k)} + \frac{\alpha_2(k)}{\omega - \omega_2(k)} \tag{3.18}$$

In comparison with the atomic limit, where the Green's function has two δ-peaks, one sees that the Green's function 3.18 corresponds to two bands described by $\omega_1(k)$ and $\omega_2(k)$.

3.2 Cluster perturbation theory: an improved Hubbard-I approximation

The idea of the cluster perturbation theory (CPT) [12, 21, 14] is to divide the whole lattice into identical clusters, forming a superlattice (see Fig. 3.1). So in the Hubbard Hamiltonian one separates the hopping into those between different atomic sites in one cluster and those in between different clusters.

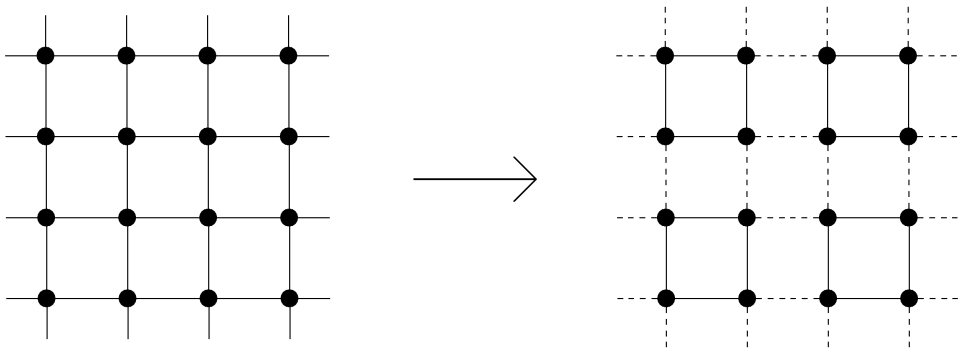

Figure 3.1: The Tiling of the lattice into identical clusters. The solid lines indicate hoppings within one cluster and the dashed lines the hopping between different clusters.

Thus, the hopping matrix t, a matrix in site indices which describes the hoppings in the original lattice, is splitted in the following way:

$$t = \begin{pmatrix} \tilde{t}' & \tilde{T} \\ \tilde{T} & \tilde{t}' \end{pmatrix} = \underbrace{\begin{pmatrix} \tilde{t}' & 0 \\ 0 & \tilde{t}' \end{pmatrix}}_{t'} + \underbrace{\begin{pmatrix} 0 & \tilde{T} \\ \tilde{T} & 0 \end{pmatrix}}_{T} \tag{3.19}$$

where t' denotes the hoppings within a single (isolated) cluster and T the intercluster hoppings between different clusters. So one can write the relation:

$$t = t' + T \tag{3.20}$$

This means, that one can write the Hamiltonian H of the full lattice (Eq. 3.2) in the following form

$$H = \underbrace{H_0(t') + H_1(U)}_{H_{cluster}} + H_0(T), \tag{3.21}$$

where H_0 is the (now splitted) hopping term and H_1 is the interaction term of the Hubbard model. $H_{cluster}$ denotes the Hamiltanian for the cluster only.

In order to calculate the Green's function of the whole lattice $G(\omega)$ the Dyson equation is used

$$G^{-1}(\omega) = G_0^{-1}(\omega) - \Sigma(\omega), \tag{3.22}$$

where again the self energy $\Sigma(\omega)$ has to be determined. In contrary to the Hubbard-I approximation, one now approximates this with the self energy of an isolated cluster $\Sigma_{cluster}(\omega)$:

$$\Sigma(\omega) \cong \Sigma_{cluster}(\omega) \tag{3.23}$$

since here short range hoppings t' in the cluster are considered, this means an improvement with respect to the Hubbard-I approximation, where no hoppings at all were considered (atomic limit) for Σ.

So the cluster self energy

$$\begin{aligned} \Sigma_{cluster}(\omega) &= \left(G^{(0)}_{cluster}(\omega)\right)^{-1} - \left(G_{cluster}(\omega)\right)^{-1} \\ &= -\left(\omega + \mu - t'\right) + \left(G_{cluster}(\omega)\right)^{-1} \end{aligned} \tag{3.24}$$

is used to calculate the lattice Green's function

$$\begin{aligned} G(\omega) &= \frac{1}{G_0^{-1}(\omega) - \Sigma_{cluster}(\omega)} \qquad (3.25) \\ &= \frac{1}{(\omega+\mu-t) - (\omega+\mu-t') + (G_{cluster}(\omega))^{-1}} \\ &= \frac{1}{(G_{cluster}(\omega))^{-1} - t + t'} \\ G(\omega) &= \frac{1}{(G_{cluster}(\omega))^{-1} - T} \qquad (3.26) \end{aligned}$$

3.2.1 CPT by hand

To illustrate the cluster perturbation theory technique we will calculate by hand a simple example. We consider a single-band Hubbard model on one-dimensional lattice decomposed into clusters containing two sites. Thus, we have the effective spatial indices of 1 and 2. In this way we can write the cluster Green's function in real space in the following matrix form:

$$G_{ij}^{cluster} = \begin{pmatrix} G_{11} & G_{12} \\ G_{21} & G_{22} \end{pmatrix} \qquad (3.27)$$

For simplicity of the calculation, we consider here the non-interacting limit of the Hubbard Hamiltonian, i.e. the $U = 0$ case only. So the Green's function in k-space reads:

$$G(k,\omega) = \frac{1}{\omega - \epsilon(k)} \quad \text{with} \quad \epsilon(k) = -t\cos k \qquad (3.28)$$

The cluster Green's function in real space is then obtained by Fourier transformation

$$G_{cluster}^{(i,j)} = \frac{1}{2}\sum_k G(k,\omega) e^{ik(r_i - r_j)} \quad ; \quad k = 0, \pi \qquad (3.29)$$

where the sum is over all (two) possible k within one cluster. Thus the normalization factor is 1/2.

We now can compute in real space

$$G_{11} = \frac{1}{2}\left(\frac{1}{\omega - \epsilon(0)} + \frac{1}{\omega - \epsilon(\pi)}\right) = \frac{1}{2}\left(\frac{1}{\omega + t} + \frac{1}{\omega - t}\right), \tag{3.30}$$

$$G_{12} = \frac{1}{2}\left(\frac{1}{\omega - \epsilon(0)} + \frac{1}{\omega - \epsilon(\pi)}e^{-i\pi}\right) = \frac{1}{2}\left(\frac{1}{\omega + t} - \frac{1}{\omega - t}\right), \tag{3.31}$$

$$G_{21} = \frac{1}{2}\left(\frac{1}{\omega - \epsilon(0)} + \frac{1}{\omega - \epsilon(\pi)}e^{+i\pi}\right) = \frac{1}{2}\left(\frac{1}{\omega + t} - \frac{1}{\omega - t}\right), \tag{3.32}$$

$$G_{22} = G_{11}, \tag{3.33}$$

which leads to

$$G^{ij} = \frac{1}{\omega^2 - t^2}\begin{pmatrix} \omega & -t \\ -t & \omega \end{pmatrix} \tag{3.34}$$

and finally

$$\left(G^{ij}\right)^{-1} = \begin{pmatrix} \omega & t \\ t & \omega \end{pmatrix}. \tag{3.35}$$

In order to combine all the clusters forming the lattice, we have to calculate the intercluster hopping T. We define a superlattice, which contains one cluster at each superlattice point. The translation vector in this superlattice is $a = 2$ in units of the original lattice. The corresponding reciprocal vector is denoted Q (in the reciprocal superlattice space). Δ is the distance between two clusters, give in original lattice units $\Delta = +2, -2$. The intercluster hopping matrix T is then

$$T^{ij}(Q) = \sum_{superlattice} -t_{ij}e^{-iQ(R_A - R_B)}, \tag{3.36}$$

where the indices ij denote different atomic sites (in the sense of the original lattice) and A, B denote different clusters (as index of the superlattice). Since the intercluster hopping just takes place between neighbor clusters, the sum condenses in fact to just one Fourier component. So we can calculate

$$T^{12}(Q) = (-t)e^{-iQ(+2)} = -te^{-2iQ} \tag{3.37}$$

$$T^{21}(Q) = (-t)e^{-iQ(-2)} = -te^{+2iQ} \tag{3.38}$$

$T^{11} = T^{22} = 0$ since intercluster hopping just takes place between the edges of two clusters. We then get

$$T^{ij}(Q) = \begin{pmatrix} 0 & -te^{-2iQ} \\ -te^{+2iQ} & 0 \end{pmatrix} \tag{3.39}$$

In order to derive the Green's function for the whole lattice G^{ij}_{CPT}, we insert the obtained results for $G_{cluster}$ (Eq. 3.35) and T (Eq. 3.39) into the CPT equation (3.26).

$$\left(G^{ij}_{CPT}\right)^{-1}(Q,\omega) = \left(G^{ij}_{cluster}\right)^{-1} - T(Q) \tag{3.40}$$

$$= \begin{pmatrix} \omega & t + te^{-2iQ} \\ t + te^{+2iQ} & \omega \end{pmatrix}$$

$$= \begin{pmatrix} \omega & 2te^{-iQ}\cos Q \\ 2te^{+iQ}\cos Q & \omega \end{pmatrix}. \tag{3.41}$$

Inverting yields

$$G^{ij}_{CPT}(Q,\omega) = \frac{1}{\omega^2 - 4t^2\cos^2 Q} \begin{pmatrix} \omega & -2te^{-iQ}\cos Q \\ -2te^{+iQ}\cos Q & \omega \end{pmatrix}, \tag{3.42}$$

which can also be written in the following form

$$G^{ij}_{CPT}(Q,\omega) = \frac{1}{2} \begin{pmatrix} \frac{1}{\omega-2t\cos Q} + \frac{1}{\omega+2t\cos Q} & e^{-iQ}\left(\frac{1}{\omega+2t\cos Q} - \frac{1}{\omega-2t\cos Q}\right) \\ e^{iQ}\left(\frac{1}{\omega+2t\cos Q} - \frac{1}{\omega-2t\cos Q}\right) & \frac{1}{\omega-2t\cos Q} + \frac{1}{\omega+2t\cos Q} \end{pmatrix} \tag{3.43}$$

This Green's function is still in a mixed representation, ij and Q. We obtain the representation in full momentum space by Fourier transformation

$$G_{CPT}(Q,\omega) = \frac{1}{N}\sum_{ij} G^{ij}_{CPT}(Q,\omega)e^{-iQ(r_i - r_j)} \tag{3.44}$$

$$= \frac{1}{2}\left(G^{11}_{CPT} + G^{12}_{CPT}e^{iQ} + G^{21}_{CPT}e^{-iQ} + G^{22}_{CPT}\right)$$

$$= \frac{1}{4}\frac{4}{\omega + 2t\cos Q} \tag{3.45}$$

So we obtain the final result

$$\begin{aligned} G_{CPT}(\omega, Q) &= \tfrac{1}{\omega - \epsilon(Q)} \\ \epsilon(Q) &= -2t \cos Q \end{aligned} \tag{3.46}$$

This result gives the dispersion $\epsilon(Q)$ for the case of non-interacting electrons ($U = 0$), for which the CPT method yields the exact solution.

3.3 The Variational Cluster Approach

The CPT method yields good results in many cases, but cannot describe symmetry broken phases, since there is no self consistent procedure involved. The method presented in this section (following mainly [22]), the so called Variational Cluster Perturbation Theory is a variational extension of CPT and overcomes this limitation.

We recall the equation for the full Hamiltonian in the CPT:

$$H = \sum_R \underbrace{\left(H_0^{cluster} + H_1(R)\right)}_{H^{cluster}} + \sum_{R,R'} H_0^i(R, R'), \tag{3.47}$$

where to the Hamiltonian describing the cluster, the term H_0^i which describes the hopping between different clusters, is added as a perturbation. But in fact, this perturbation term need not necessarily to be restricted to the inter-cluster hopping term, but could be any single-particle operator. This means that the decoupled Hamiltonian (3.47) is invariant under the transformation

$$\begin{aligned} H_0^{cluster}(R) &\to H_0^{cluster}(R) + H'(R) \\ H_0^i(R, R') &\to H_0^i(R, R') - \delta_{R,R'} H'(R) \end{aligned} \tag{3.48}$$

with an arbitrary intra-cluster single-particle operator

$$H'(R) = \sum_{i,j} \Delta_{i,j} c_{R,i}^\dagger c_{R,j} \tag{3.49}$$

with i, j general single-particle quantum numbers in the cluster. In terms of CPT this means that a one particle operator is added to the cluster Hamiltonian and substracted again perturbatively.

The reason for including additional terms is that one may think of choosing the parameters Δ such that the single-particle dynamics of the cluster problem is as close as possible to the exact dynamics of the whole lattice.

To specify this, one considers a thermodynamical function, e.g. the grand potential Ω, and search for a stationary point with respect to δ. The so called Self-Energy-Functional Approach (SFA) [15, 16, 13] yields the form

$$\Omega\left(\Sigma^{cl}\right) = \Omega^{cl} + Tr\ln\left(-(G_0^{-1} - \Sigma_{cl}^{-1})\right) - Tr\ln\left(-G^{cl}\right) \tag{3.50}$$

$$= \Omega^{cl} + Tr\ln\left(-G\right) - Tr\ln\left(-G^{cl}\right) \tag{3.51}$$

where Ω^{cl}, G^{cl} and Σ^{cl} are the grand potential, the Green's function and the self energy of the cluster, whereas G_0 and G are the free and the interacting Greens function of the lattice, respectively.

Depending on the problem under consideration, the additional one particle operator Eq. (3.49) can be chosen to represent different external fields. For the following application of the VCA method to $SrVO_3$ we restrict to the chemical potential μ as variational parameter. The results of this calculation are presented in chapter 4.

Chapter 4

Correlation effects in $SrVO_3$: an LDA + VCA study

The family of prevovskite $SrMO_3$, where M is a $3d$-metal, attracts a lot of attention in material science because of its interesting combined electronic, magnetic and transport properties. Among these perovskites, some attention is given to the $SrVO_3$ which is a $3d^1$- metal, in particular this cubic structure is treated as a model system for discussing correlation effects [23, 24]. From a theoretical point of view, the electronic structure description is still an area of active research, and there are a large number of publications such as the LCAO-based, as well as full-potential LAPW or linear muffin tin orbitals (LMTO) or pseudopotentials, ab-initio band structure calculations.

This chapter presents results using the LDA+VCA approach to describe electron correlations in $SrVO_3$. We analyze the results and compare them with recent theoretical LDA+DMFT data, as well as with experimental PES measurements. In the first section we discuss the crystal and electronic structure as obtained from an ab-initio LSDA description. Based on these results, we identify that the three Vanadium$-3d(t_{2g})$ orbitals play the crucial role in this compound.

In the following section, we construct the real-space Hamiltonian for these $V(t_{2g})$ orbitals using the downfolding technique within the NMTO formalism. This provides us the hopping parameters for the low-energy model Hamiltonian. Finally, to this non-interacting Hamiltonian, we add the interaction part by introducing U and form the three-orbital Hubbard Hamiltonian.

In the third section of this chapter, we solve this interacting three-band

Hubbard model Hamiltonian using the many-body Variational Cluster Approach (VCA). We perform the calculations for different cluster geometries and different values for the on-site Coulomb parameter U. The results are discussed and the conclusions are presented at the end of this chapter.

4.1 Crystal and electronic structure of $SrVO_3$

The transition metal compound $SrVO_3$ is of Perovskite type and has an ideal cubic structure with the space group $Pm-3m$. Its crystal structure is illustrated in Fig. 4.1. The positions of the atoms in the elementary cell are $(0,0,0)$ for Vanadium in the (1a) site, (1/2, 1/2, 1/2) for Strontium in the (1b) site and Oxygen occupies the (3d) site situated at $(0,0,1/2)$. Each Vanadium atom is surrounded by six Oxygen atoms forming an octahedron. The atomic electronic configurations for the constituents of this compound are $[Ar]3d^3 4s^2$ for V, $[Kr]5s^2$ for Sr, and $[He]2s^2 2p^4$ for O.

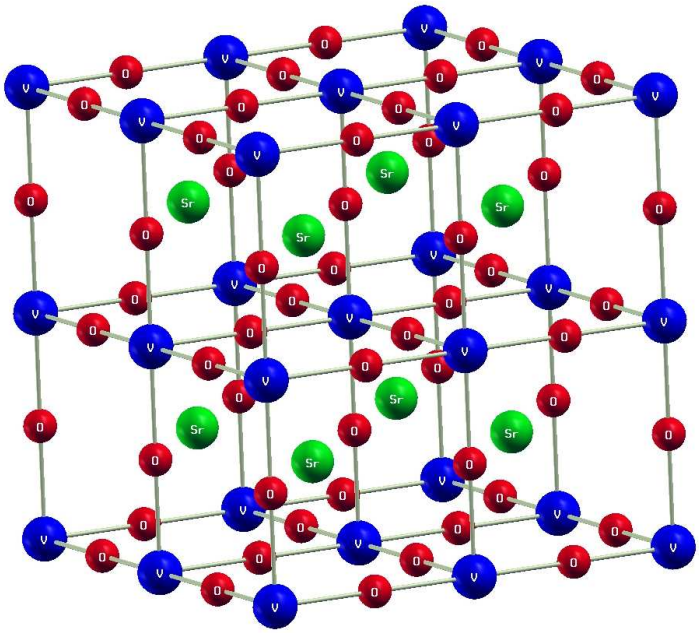

Figure 4.1: Crystal structure for $SrVO_3$ forming an ideal cubic structure. Blue spheres represent Vanadium, green spheres Strontium and red spheres Oxygen atoms.

We performed the band structure calculations using the Stuttgart TB-LMTO47 computer program code[25]. The exchange correlation potential was treated by the Local Density Approximation (LDA), and a scalar relativistic scheme was used for the valence electrons. The lattice constant was assumed to be $a = 7.26 a.u.$, and self-consistency calculation was iterated until the difference in the total energy was less then $10^{-6} Ry$. The density of states was obtained by using a modified tetrahedron method.

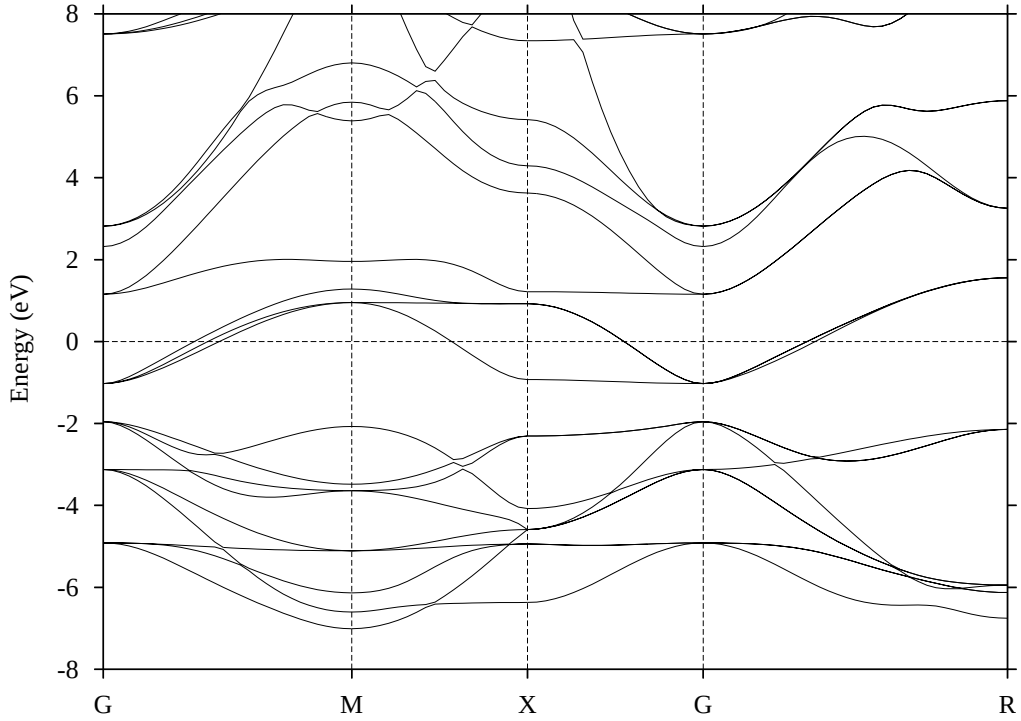

Figure 4.2: The LDA band structure for cubic $SrVO_3$. The $V - 3d$ states are situated at the Fermi level (see also Fig. 4.3).

In Fig. 4.2 the dispersion curves $E(k)$ along some high-symmetry points of the Brillouin zone are represented in a large energy range of $\pm 8eV$ around the Fermi Energy. The lower bands between -7 and $-2eV$ contain $Sr - 5s$ and $O - 2p$ states and they form the upper valence band with a width of about $5eV$. Some admixture of V states also present. The bottom of the conducting band around the Fermi level is composed mainly of $V - 3d(t_{2g})$-orbtials and $V - 3d(e_g)$, but also little admixture of $O - 2p$ states contribute in this range. At higher energy range the $Sr - 4d$-like bands are placed.

As one can see from the crystal structure, the Vanadium ion is octahedraly surrounded by six oxygen ions. The octahedral crystal field splits the $V-3d$ states according to their symmetries into t_{2g} and e_g orbitals. Since in the cubic symmetry the hybridization between t_{2g} and e_g is forbidden, the orbitals in both subbands are degenerate.

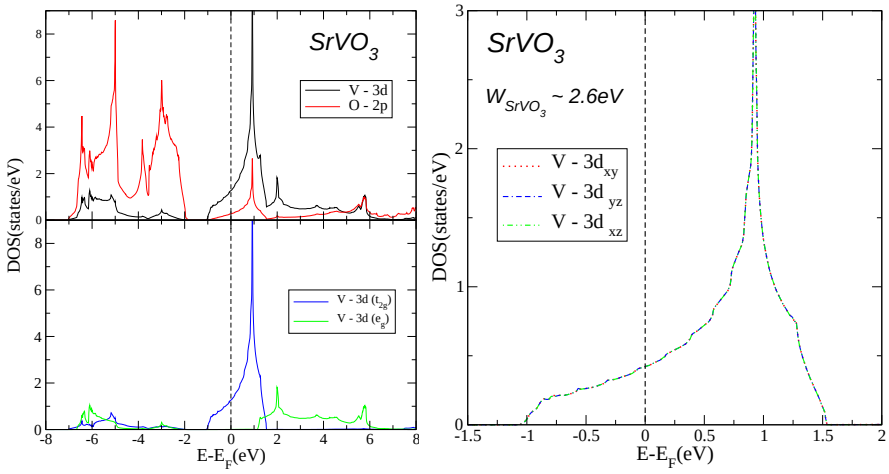

Figure 4.3: LDA density of states (DOS) for $SrVO_3$ as calcualted by the LMTO. Left: The upper panel shows the $V-3d$ and $O-2p$ contributions and the lower panel shows the partial density of states for the t_{2g} and e_g orbitals of the $V-3d$ states. Right: The t_{2g} only contribution to the Density of states, which has a bandwidth of $2.6eV$ in the energy range of interest around the Fermi energy E_F.

The calculated total and partial densities of states are shown in Fig. 4.3. The total density of states is almost entirely composed of $V-3d$ and $O-2p$ states. In the energy range between -7 and $-2eV$, the $O-2p$ states are dominant, while around $-1eV$ and above, the $V-3d$ states have the most spectral weight. In the lower left panel of Fig. 4.3, the $V-3d$ states are decomposed into t_{2g} and e_g orbitals. Below the Fermi level both t_{2g} and e_g states have a small spectral weight, and around the Fermi energy E_F the t_{2g} contribution is essential.

Since the important physics of electrons takes place near the Fermi energy, we now have learned by the above LDA bandstructure calculations which

orbitals are of interest in this $SrVO_3$ compound. We find a bandwidth of about $2.6eV$ for the $V-3d(t_{2g})$-states crossing the Fermi energy. Thus, these orbitals should be taken into account in a many body calculation. In order to do that, we have to derive a low-energy Hamiltonian for these states. This will be discussed in the following section.

4.2 Model Hamiltonian for the t_{2g} orbitals

After having identified the $V-3d-t_{2g}$ orbitals as the ones of interest in the $SrVO_3$ material, we now want to construct a model Hamiltonian restricted to these three bands only. For this purpose, we downfold the full bandstructure obtained by LDA in the previous section to the $V-t_{2g}$ orbitals. This is done using the Nth order muffin tin orbital (NMTO) method (see section 2.1) in the Stuttgart-NMTO program [4, 6]. By massive downfolding, this approach generates a minimal basis set of symmetrically orthonormalized NMTO's forming a set of localized Wannier functions. The result of this downfolding calculation is shown in Fig. 4.4. For the present calculation we use energy mesh points ϵ_ν of 0.4 and $1.3eV$. We observe a rather good agreement with the bandstructure of the full basis obtained by LDA.

By Fourier transformation of the orthonormalized NMTO Hamiltonian, $H^{\mathrm{LDA}}(\mathbf{k})$, we obtain the real-space Hamiltonian, yielding on-site energies and hopping integrals,

$$H^{NMTO}_{\mathbf{R}'m',\mathbf{R}m} \equiv \left\langle \chi^{\perp}_{\mathbf{R}'\,m'} \left| H^{LDA} - \varepsilon_F \right| \chi^{\perp}_{\mathbf{R}\,m} \right\rangle \equiv t^{\mathbf{\Delta}}_{m',m}, \tag{4.1}$$

in the Wannier representation $\chi^{\perp}_{\mathbf{R}m}$. The matrix element between orbitals m' and m, both on site $\mathbf{R}'$=$\mathbf{R}$, is $t^{\mathbf{0}}_{m',m}$, and the hopping integral from orbital m' on site $\mathbf{R}'$ to orbital m on site $\mathbf{R}$ is $t^{\mathbf{\Delta}}_{m',m}$, with $\mathbf{\Delta} = \mathbf{R} - \mathbf{R}'$.

The one-particle Hamiltonian matrix elements are presented below. We use the convention in which $m = 1, 2, 3$ corresponds to the t_{2g}-subset of the V-d orbitals in the following order: $\{d_{xy}, d_{yz}, d_{zx}\}$. The matrix elements for the on-site energies $\epsilon_m \equiv t^{\mathbf{0}}_{m,m}$ are obtained to be

$$\epsilon^{\mathrm{V}}_m = (-1433, -1433, -1433)\,, \tag{4.2}$$

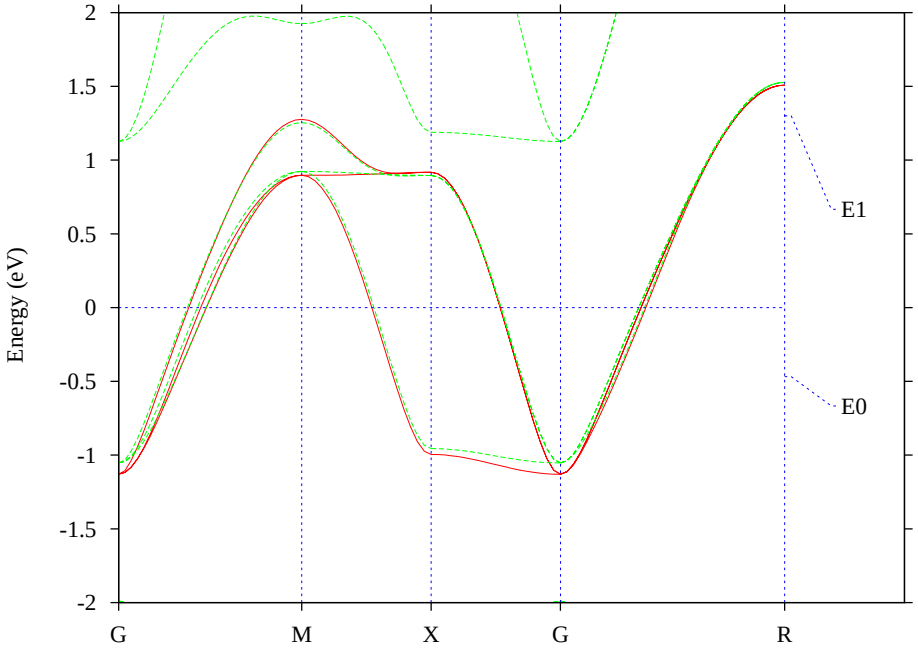

Figure 4.4: The NMTO downfolded t_{2g}-bands (red line) in comparison with the full LDA bands (green line).

For the nearest-neighbor hopping terms with $\mathbf{\Delta_1} \equiv (1,0,0)$ we obtain

$$t^{\mathbf{\Delta_1}}_{m',m} = \begin{pmatrix} -270 & 0 & 0 \\ 0 & -31 & 0 \\ 0 & 0 & -270 \end{pmatrix} , \tag{4.3}$$

and for the second-nearest-neighbor terms with $\mathbf{\Delta_2} \equiv (1,1,0)$

$$t^{\mathbf{\Delta_2}}_{m',m} = \begin{pmatrix} -88 & 0 & 0 \\ 0 & 7 & 5 \\ 0 & 5 & 7 \end{pmatrix} , \tag{4.4}$$

Here, all hoppings are given in units of meV, and only one representative hopping integral is shown for each class. Other hopping terms can be derived from proper unitary transformation using crystal symmetry (see, e.g., Ref. [23] for details). As one can see from Eq. (4.3), the largest hoppings follow the symmetry of the orbital in question, e.g. the d_{xy} and the d_{zx}-orbitals show large hopping amplitudes along the x-direction. In addition, there

are further hopping terms in the Hamiltonian, which we don't show here for simplicity. We have taken into account hoppings up to a range of $r = 2.7a$. Neglected hoppings are more than a factor 1000 smaller than the largest nearest-neighbor hopping. The non-interacting part of the effective Hamiltonian for $SrVO_3$, thus, has the form

$$H_0^{LDA} = \sum_{\mathbf{R}',\mathbf{R},\sigma} \sum_{\{m',m\}} t_{m',m}^{\mathbf{R}'-\mathbf{R}} c^\dagger_{\mathbf{R}'m'\sigma} c_{\mathbf{R}m\sigma}. \tag{4.5}$$

The many-body hamiltonian contains the hopping part described within the LDA, H_0^{LDA} to which the interacting part is added, such that the total Hamiltonian can be written as:

$$H = H_0^{LDA} + H_{int} \tag{4.6}$$

The interaction part H_{int} takes into account the correlation effects and is written as

$$\begin{aligned} H_{int} &= \sum_{\mathbf{R},m} U n_{\mathbf{R}m\uparrow} n_{\mathbf{R}m\downarrow} \\ &+ \sum_{\mathbf{R},m<m',\sigma,\sigma'} (U' - J\delta_{\sigma,\sigma'}) n_{\mathbf{R}m\sigma} n_{\mathbf{R}m'\sigma'} \\ &+ \sum_{\mathbf{R},m<m'} J c^\dagger_{\mathbf{R}m'\uparrow} c^\dagger_{\mathbf{R}m\downarrow} c_{\mathbf{R}m'\downarrow} c_{\mathbf{R}m\uparrow} + \text{h.c.} \\ &+ \sum_{\mathbf{R},m<m'} J c^\dagger_{\mathbf{R}m'\uparrow} c^\dagger_{\mathbf{R}m'\downarrow} c_{\mathbf{R}m\downarrow} c_{\mathbf{R}m\uparrow} + \text{h.c.}, \end{aligned} \tag{4.7}$$

where U and U' denote the Coulomb-interactions and J the Hund's rule coupling constant. In Eqs. (4.5) and (4.7), $c_{\mathbf{R}m\sigma}$ ($c^\dagger_{\mathbf{R}m\sigma}$) are the usual fermionic annihilation (creation) operators acting on an electron with spin σ at site $\mathbf{R}$ in the orbital m. The third and fourth term in 4.7 are describing the spin-flip and the pair-flip of two electrons.

In order to determine all possible local Coulomb interactions between two electrons with spin σ' and σ in the orbitals m' and m on the same atomic

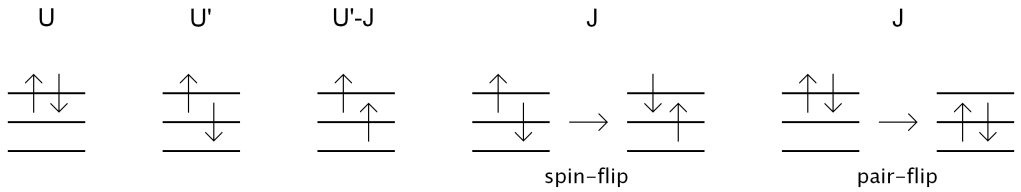

Figure 4.5: The Coulomb interactions U taken into account in H_{int}

site, we can introduce an interaction matrix $\mathcal{U}^{\sigma'\sigma}_{m'm}$ (see Fig. 4.5).

$$\mathcal{U}^{\sigma'\sigma}_{m'm} = \begin{array}{c|cccccc} & m_0\uparrow & m_1\uparrow & m_2\uparrow & m_0\downarrow & m_1\downarrow & m_2\downarrow \\ \hline m_0\uparrow & 0 & U'-J & U'-J & U & U' & U' \\ m_1\uparrow & U'-J & 0 & U'-J & U' & U & U' \\ m_2\uparrow & U'-J & U'-J & 0 & U' & U' & U \\ m_0\downarrow & U & U' & U' & 0 & U'-J & U'-J \\ m_1\downarrow & U' & U & U' & U'-J & 0 & U'-J \\ m_2\downarrow & U' & U' & U & U'-J & U'-J & 0 \end{array} \tag{4.8}$$

Here, U is the interaction between two electrons with different spin on the same orbital, U' and $U'-J$ are the interactions for electrons in different orbitals with antiparallel and parallel spin respectively. We have the following simple relations for these values

$$\begin{aligned} U' &= U - 2J \\ U' - J &= U - 3J \end{aligned} \tag{4.9}$$

The strengths of the local interactions can be calculated by means of the constrained LDA method [26, 27], allowing the e_g states to participate in screening [28, 29]. Therefore, a value for $U = 5.5eV$ can be found, which motivates the choice of the considered values for U in the range of 4 to $6eV$ in the following numerical calculations. The Hund's coupling constant is assumed to be $J = 1eV$ [29].

4.3 Correlation effects: Variational Cluster Approach

In the previous section we have derived an effective model Hamiltonian which describes our problem, that we now are going to solve. This is done

by the Variational Cluster Approach, which was introduced in section 3.3 [12, 30, 13, 17].

First of all, we have to determine the cluster for the calculations, more specifically, we need its geometrical shape and its size. The choice of the clusters must be in a way, that they fill the whole lattice space by transformation with suitable translation vectors. The model will be solved exactly within these clusters, whereas the hoppings between these clusters are treated perturbatively. Self consistency is achieved within the VCA by taking the chemical potential μ as a variational parameter.

We consider three different types of cluster, presented in Fig. 4.6.

- Cluster 1: A cluster containing two sites in z-direction. The corresponding translation vectors are $(1,0,0)$, $(0,1,0)$, and $(0,0,2)$
- Cluster 2: A cluster containing four sites in a quadratic form in the x,z-plane, with translation vectors $(2,0,0)$, $(0,1,0)$, and $(0,0,2)$
- Cluster 3: A cluster containing four sites on the spatial axes forming a tetragon. The whole lattice space is filled with the translation vectors $(2,0,0)$, $(0,0,2)$, and $(1,1,1)$. Obviously this cluster is isotropic.

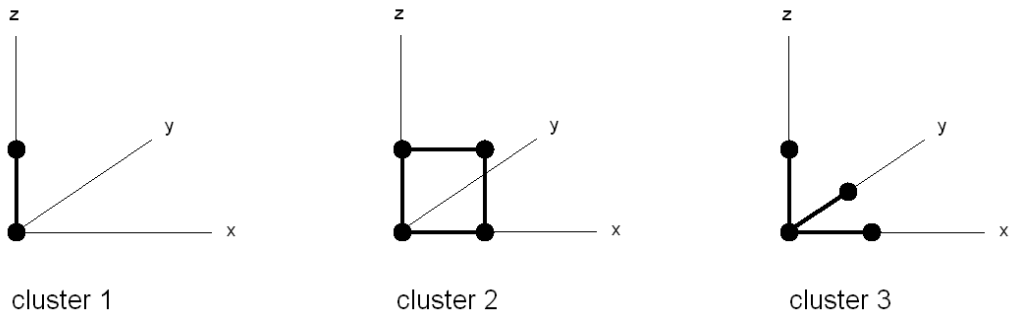

Figure 4.6: The different cluster geometries taken into account.

We performed the calculations for all three cluster types and for different particle sectors (number of particles with spin up and spin down) in the clusters, such as the 1-1, 2-2 and 3-3.

The resulting density of states (DOS) of these calculations is shown in Fig. 4.7. The interaction parameter was assumed to be $U = 5.55eV$. For the cluster 1, the results show that two orbitals are preferentially occupied, while the remaining third orbital is empty. This demonstrates that cluster geometry breaks the degeneracy of the t_{2g}-orbitals. The situation is similar in cluster 2, where also no equal occupation is achieved for the three t_{2g}-orbitals. That is why we consider for the following the isotropic cluster 3, for which the 2-2 particle sector corresponds to the realistic description.

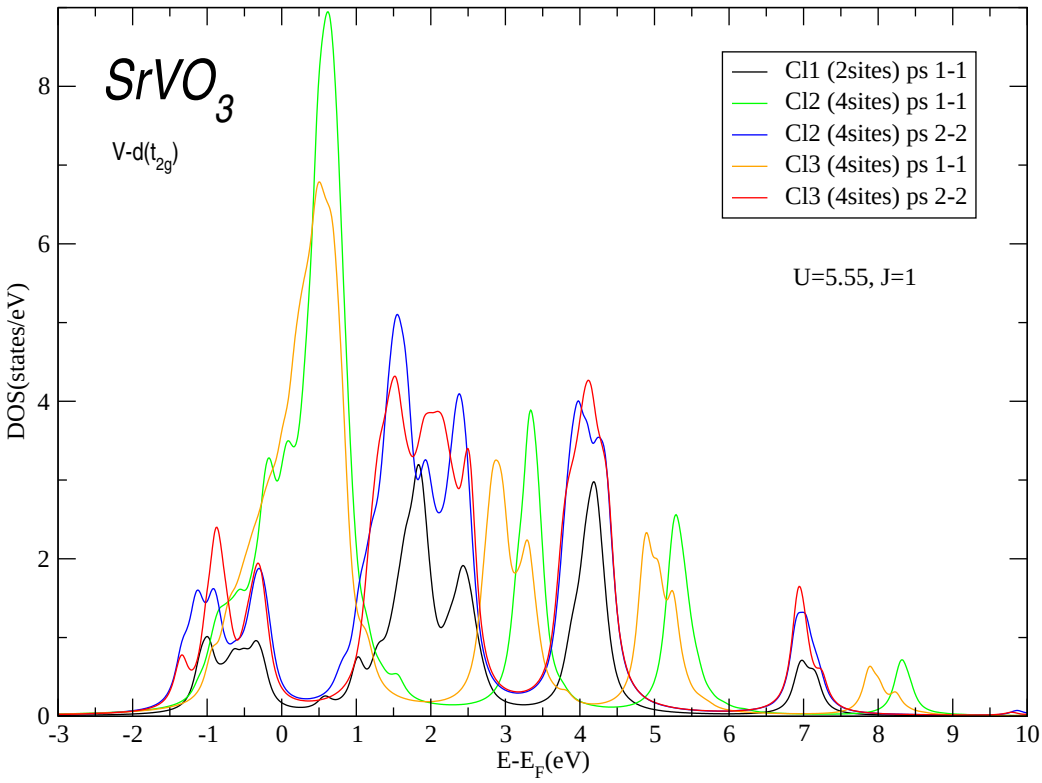

Figure 4.7: Density of states for the LDA+VCA calculations for different cluster geometries and occupations.

Having chosen the best cluster, the cluster 3, we investigate the dependence of the results on different values of the interaction parameter U. In Fig. 4.8 the results of DOS for different values of U are presented.

We can observe a behavior typical for a material close to the metal-

insulator transition. For a value of $U = 4eV$ the figure shows a metallic density of states, and a little change of the on-site Coulomb parameter to a value of $4.25eV$ determines the appearance of a pseudo-gap at the Fermi level. Increasing further the value of U, the density of states are continuously depleted, such that already at $U = 6eV$ there is a large energy distance to the next states situated at about $2eV$. This indicates that the system reached the insulating state.

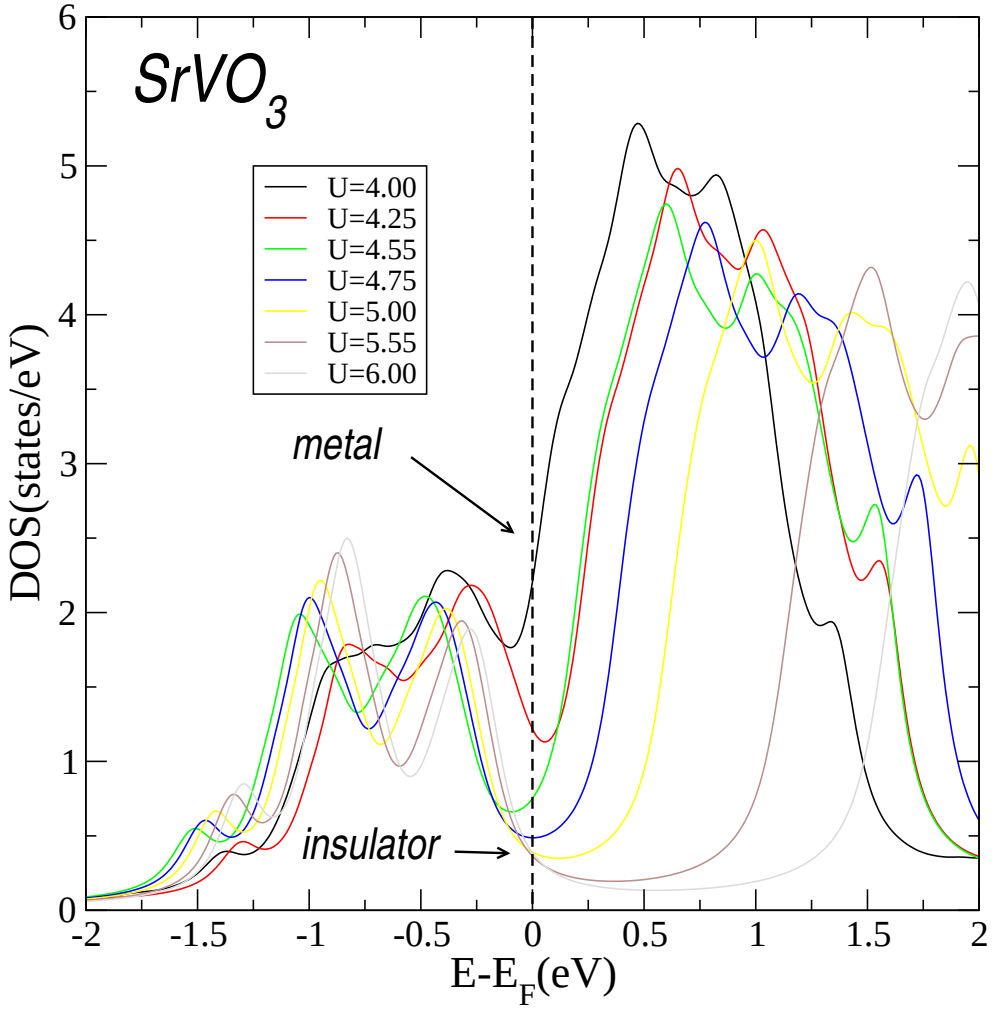

Figure 4.8: Density of states of $SrVO_3$ for different values of the interaction parameter U. We observe a metal to insulator transition for increasing U.

In Fig. 4.9 we compare the LDA+VCA results with previous calculations using Dynamical Mean Field Theory (DMFT) and with experimental measurements obtained by photoemission spectroscopy (PES).

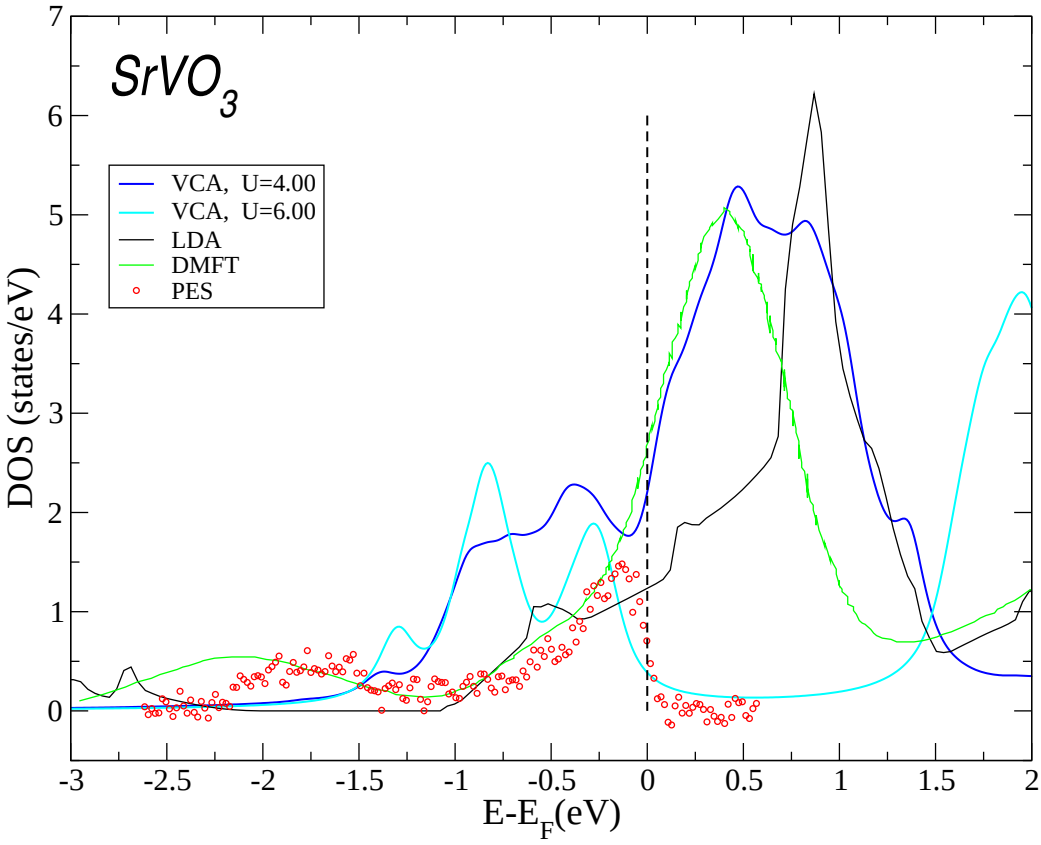

Figure 4.9: Comparison of results obtained with different methods, i.e. LDA, LDA+VCA, LDA+DMFT [32], and with experimental PES measurements [24].

Previous LDA+DMFT calculations have been performed using the Quantum Monte Carlo solver and the Maximum Entropy Method to extract the density of states [31, 32]. In the LDA+DMFT calculations [32], the k-resolved spectral function shows the presence of the Lower and the Upper Hubbard band and the quasiparticle band close to the Fermi level. In the density of states, the Lower Hubbard band is centered about $-2eV$, the maximum of the quasiparticle peak is centered about $0.5eV$ above the Fermi level, and the Upper Hubbard band is situated at about $3eV$.

The experimental data were extracted from the work of Sekiyama et al. [24], obtained by PES measurements. The LDA+DMFT results and the experimental spectra compare very well. These results demonstrate that $SrVO_3$ is a strongly correlated metal but not on the border of the Mott-Hubbard metal-insulator transition. The differences between the computed LDA+DMFT results and the experimental spectra are explained due to some uncertainties in the ab-inito calculations for the Coulomb parameter and the specific treatment of the experimental data to extract the d-electrons spectra.

The LDA+VCA results, do not compare well with the LDA+DMFT calculations. Both calculations use the same downfolding procedure, with very similar results. Therefore the difference can only be attributed to the different treatment of the many-body problem. The LDA+VCA density of states results show the Lower Hubbard band at around $-0.75eV$ and an Upper Hubbard band centered around $0.5eV$. As the values for U are increased, the Lower Hubbard band is maintaining its position, while the upper Hubbard band is gradually shifted to higher energies. No clear quasiparticle states are evidenced. A possible explanation of the discrepancy could be connected with the different dynamics which is captured in DMFT in comparison with VCA.

Chapter 5

Conclusion

In this diploma work we created a code to implement the Löwdin downfolding method [6]. By effectively integrating out some of the orbitals, this method generates effective low-energy Hamiltonians in a reduced Hilbert space. We applied this method to different tight-binding multi-band models for CuO_2 planes in High Temperature Superconductor materials.

We have seen that the accuracy of this method, in which the effective reduced model describes the initial full one, depends strongly on the energy mesh used in the calculation. These parameters have to be chosen appropriately 'by experience', which is of course a certain drawback of this method. The energy mesh points have to lie in the region around the downfolded bands to get a good result. When possible, they should not be chosen close to energies of other bands where hybridization with the remaining orbitals is significant. Furthermore, an increasing number of mesh-points increases the accuracy, provided that they lie in a reasonable region. The calculations yield good results even for just two or three energy mesh points.

It would have been interesting to investigate also interacting models with the developed downfolding program. This remains to be done in the future.

In a second part of this thesis, we used the downfolding technique in the ab-initio framework of the Stuttgart NMTO package to create a minimal Hubbard-Hamiltonian to describe the physics of the correlated material $SrVO_3$ within the LDA+VCA approach.

In this $3d^1$ system, we identified the three $V-3d(t_{2g})$ orbitals as the ones responsible for the important physics. We find out that for the VCA calculation an isotropic four-site cluster does not break the degeneracy of the

orbitals and is thus a good choice.

By varying the interaction parameter U, we see that $SrVO_3$ is close to the metal-insulator transition. The results of the LDA+VCA calculation deviate from the PES experimental data. There are also differences with LDA+DMFT results, which could be explained by the different dynamics captured in this method.

Acknowledgements

I thank Prof. Dr. Enrico Arrigoni for the supervision of this thesis and for his patience and friendliness.

Great thanks I owe to DDr. Liviu Chioncel for his extensive support and encouragements and for every drink we had. He spared no effort to help me and motivated me in every possible way.

Many thanks go to DI Hannes Allmaier for his help and for introducing me to the VCA program.

I also thank Dr. Xiancong Lu, it was enjoyable to share the office with him and a pleasure to have discussions.

List of Figures

Bibliography

[1] P.-O. Löwdin, The Journal of Chemical Physics **19**, 1396 (1951).

[2] P. W. Anderson, Science **235**, 1196 (1987).

[3] O. K. Andersen, A. I. Liechtenstein, O. Jepsen, and F. Paulsen, J. Phys. Chem. Solids **56**, 1573 (1995).

[4] O. K. Andersen and T. Saha-Dasgupta, Phys. Rev. B **62**, R16219 (2000).

[5] O. K. Andersen *et al.*, Psi-k Newsletter **45**, 86 (2001).

[6] E. Zurek, O. Jepsen, and O. K. Andersen, ChemPhysChem **6**, 1934 (2005).

[7] O. K. Andersen, T. Saha-Dasgupta, and S. Ezhov, Bull. Mater. Sci. **26**, 19 (2003).

[8] M. S. Hybertsen, M. Schlüter, and N. E. Christensen, Phys. Rev. B **39**, 9028 (1989).

[9] O. K. Andersen, O. Jepsen, A. I. Liechtenstein, and I. I. Mazin, Phys. Rev. B **49**, 4145 (1994).

[10] J. Hubbard, Proc. R. Soc. London **276**, 238 (1963).

[11] J. Hubbard, Proc. R. Soc. London **281**, 401 (1964).

[12] C. Gros and R. Valenti, Phys. Rev. B **48**, 418 (1993).

[13] M. Potthoff, M. Aichhorn, and C. Dahnken, Phys. Rev. Lett. **91**, 206402 (2003).

[14] D. Sénéchal, P. L. Lavertu, M. A. Marois, and A. M. S. Tremblay, Phys. Rev. Lett. **94**, 156404 (2005).

[15] M. Potthoff, Eur. Phys. J. B **32**, 429 (2003).

[16] M. Potthoff, Eur. Phys. J. B **36**, 335 (2003).

[17] C. Dahnken *et al.*, Phys. Rev. B **70**, 245110 (2004).

[18] W. Hanke, M. Aichhorn, E. Arrigoni, and M. Potthoff, Physica B **378–380**, 60 (2006).

[19] C. Dahnken, M. Potthoff, E. Arrigoni, and W. Hanke, in *High Performance Computing in Science and Engineering, 2004*, edited by E. Krause, W. Jäger, and M. Resch (Springer Verlag, Berlin, 2004), p. 141.

[20] F. Gebhard, *The Mott Metal-Insulator Transition - Models and Methods*, No. 137 in *Springer Tracts in Modern Physics* (Springer, Heidelberg, 1997).

[21] S. G. Ovchinnikov and I. S. Sandalov, Physica C **161**, 607 (1989).

[22] M. Aichhorn, Ordering Phenomena in Strongly-Correlated Systems: Cluster Perturbation Theory Approach, PhD thesis, Technical University Graz, 2004.

[23] E. Pavarini, A. Yamasaki, J. Nuss, and O. K. Andersen, New J. Phys. **7**, 188 (2005).

[24] A. Sekiyama *et al.*, Phys. Rev. Lett. **93**, 156402 (2004).

[25] O. K. Andersen and O. Jepsen, Phys. Rev. Lett. **53**, 2571 (1984).

[26] V. I. Anisimov and O. Gunnarsson, Phys. Rev. B **43**, 7570 (1991).

[27] K. Held *et al.*, cond-mat/001039, To appear in ijmp C in the SCES-Y2K Conference Proceedings (unpublished).

[28] V. I. Anisimov, J. Zaanen, and O. K. Andersen, Phys. Rev. B **44**, 943 (1991).

[29] F. A. Vladimir I. Anisimov and A. I. Lichtenstein, Journal of Physics: Condensed Matter **9**, 767 (1997).

[30] D. Sénéchal, D. Perez, and M. Pioro-Ladriere, Phys. Rev. Lett. **84**, 522 (2000).

[31] I. A. Nekrasov *et al.*, Eur. Phys. J. B **18**, 55 (2000).

[32] I. A. Nekrasov *et al.*, Phys. Rev. B **73**, 155112 (2006).